Decreased glutathione biosynthesis contributes to EGFR T790M-driven erlotinib resistance in non-small cell lung cancer

Hongde Li[‡#], William Stokes[¶#], Emily Chater[¶#], Rajat Roy[¶#], Elza de Bruin[§Π], Yili Hu[‡], Zhigang Liu[‡], Egbert F. Smit[&], Guus J.J.E. Heynen[※], Julian Downward[§], Michael J. Seckl[¶*], Yulan Wang[‡△],Huiru Tang[†‡*], Olivier E. Pardo[¶*]

[†] State Key Laboratory of Genetic Engineering, Ministry of Education Key Laboratory of Contemporary Anthropology, Collaborative Innovation Centre for Genetics and Development, Shanghai International Centre for Molecular Phenomics, Metabonomics and Systems Biology Laboratory, School of Life Sciences, Zhongshan Hospital, Fudan University, Shanghai 200438, China. [‡]Key Laboratory of Magnetic Resonance in Biological Systems, National Centre for Magnetic Resonance in Wuhan, State Key Laboratory of Magnetic Resonance and Atomic and Molecular Physics, Wuhan Institute of Physics and Mathematics, Chinese Academy of Sciences, Wuhan 430071, China. [¶]Division of Cancer, Department of Surgery and Cancer, Imperial College, Hammersmith Hospital, Du Cane Road, London W12 0NN, UK. [§]Signal Transduction laboratory, CRUK London Research Institute, London, WC2A 3LY, UK. [&]Dept. Pulmonary Diseases, VU University Medical Centre and [※]Section of molecular carcinogenesis, Netherlands Cancer Institute, 1066 CX Amsterdam, Netherlands. [△]Collaborative Innovation Centre for Diagnosis and Treatment of Infectious Diseases, Hangzhou 310058, China. [Π] AstraZeneca, Personalised Healthcare & Biomarkers, Molecular Diagnostics, Darwin, Building 310, Cambridge Science Park, Milton Road, Cambridge CB4 0WG, UK.

[#]These authors have contributed equally to the work.

[*]**Corresponding authors:** o.pardo@imperial.ac.uk, huiru_tang@fudan.edu.cn and m.seckl@imperial.ac.uk

Running title: GSH metabolism and erlotinib resistance

ABSTRACT

EGFR inhibitors such as erlotinib are novel effective agents in the treatment of EGFR-driven lung cancer but their clinical impact is often impaired by acquired drug-resistance through the secondary T790M-EGFR mutation. To overcome this problem, we analysed the metabonomic differences between two independent pairs of erlotinib-sensitive/resistant cells and discovered that glutathione (GSH) levels were significantly reduced in T790M-EGFR cells. We also found that Increasing GSH levels in erlotinib resistant cells re-sensitised them whereas reducing GSH levels in erlotinib sensitive cells made them resistant. Decreased transcription of the GSH-synthesising enzymes (GCLC and GSS) due to inhibition of NRF2 was responsible for low GSH levels in resistant cells that was directly linked to the T790M mutation. T790M-EGFR clinical samples also showed decreased expression of these key enzymes; increasing intra-tumoural GSH levels with a small-molecule GST inhibitor re-sensitised resistant tumours to erlotinib in mice. Thus, we identified a new resistance pathway controlled by EGFR-T790M and a therapeutic strategy to tackle this problem in the clinic.

INTRODUCTION

Lung cancer is the main cancer killer and non-small cell lung cancer (NSCLC) represents about 85% of such cases. About 10% and 30% of NSCLCs in Western and Asian populations, respectively, express an activated mutant epidermal growth factor receptor (EGFRm) and the vast majority (90%) of such patients respond to ATP-competitive EGFR tyrosine kinase inhibitors (TKIs) such as gefitinib or erlotinib [1-3]. Unfortunately, most patients can quickly acquire TKI-resistance limiting the benefits of these drugs to patients' survival.

Resistance mechanisms include Met amplification (about 5% of cases) [4] and more frequently (50% of cases) an additional T790M gatekeeper mutation within the EGFRm [5-8]. The latter enhances kinase activity by increasing the affinity of EGFR for ATP, competing out TKI binding [9]. This led to the development of compounds irreversibly interacting with EGFRm/T790M, such as afatinib, 324674 and more recently AZD9291 and CO1696 [10-12]. However, thus far clinical trials of afatinib failed to demonstrate improved response in EGFRm/T790M patients [13], and although initial trials with the irreversible inhibitor AZD9291 showed great promises, additional resistance mechanisms to these inhibitors have already surfaced [14].

Changes in cellular metabolism accompany tumourigenesis and classical chemoresistance [15-17]. Hence, changes in metabolite concentrations can specifically reflect the onset of therapy resistance, providing response/outcome biomarkers and novel therapeutic strategies to reverse resistance[18, 19]. Both ^{1}H-nuclear magnetic resonance (NMR) and mass spectrometry are efficient tools to investigate these metabolic changes [20-23] .

Here we used ^{1}H-NMR to compare the metabolic signatures of paired NSCLC cell lines expressing EGFRm without (erlotinib-sensitive) or with the additional T790M mutation (erlotinib-resistant). We showed that glutathione (GSH) levels were reduced in erlotinib-resistant NSCLC cells in a T790M-dependent manner due to decreased expression of GSH-synthesising enzymes.

Correcting this defect re-sensitised resistant cells to erlotinib *in vitro* and *in vivo*. Moreover, ethacrynic acid (EA), a glutathione-*S*-transferase inhibitor, reversed erlotinib resistance in T790M NSCLC cells *in vitro* and *in vivo* by increasing GSH levels. Since EA is a clinically-used diuretic, it could be repurposed to reverse T790M-mediated erlotinib resistance in NSCLC patients. Overall, our work demonstrated the power of metabonomic screening to generate novel research hypotheses and discover unexplored strategies to tackle drug resistance in lung cancer treatments.

RESULTS

^{1}H-NMR-based metabolic profiling reveals decreased GSH levels in erlotinib-resistant NSCLC cells

Two pairs of cell lines were employed to obtain generic metabonomic phenotypes for the erlotinib-sensitive and erlotinib-resistant NSCLC cells. The first pair were the isogenically matched PC9 (erlotinib sensitive) and PC9ER (erlotinib resistant) cells both containing ΔE746-A750 EGFRm with an additional T790M (EGFRm/T790M) mutation in PC9ER cells. The second pair included the H3255 and genetically-unrelated erlotinib-resistant H1975 cell lines sharing L858R EGFRm, but with an additional T790M mutation in the H1975. PC9ER and H1975 cells displayed significant resistance to erlotinib as compared to their sensitive counterparts **(Supplementary Figure 1A)**. This resistance was limited to EGFR TKIs as PC9ER and PC9 cells were equally sensitive to conventional chemotherapeutic agents **(Supplementary Figure 1B)**. It has been suggested that the EGFR T790M-mediated TKI resistance is due to increased affinity of the receptor for ATP which displaces competitive inhibitors such as erlotinib [24]. However, both PC9ER and H1975 showed significant resistance even to the irreversible EGFR inhibitor 324674 compared to PC9 and H3255 cells respectively **(Supplementary Figure 1C).** This clearly suggests that other unidentified molecular mechanisms also contribute to T790M-mediated TKI resistance.

To identify these, we employed ^{1}H-NMR metabonomic profiling of our erlotinib-sensitive and resistant cells. ^{1}H-NMR analysis of cell extracts from our cell lines identified 36 metabolites **(Figure 1A)** for which assignments were obtained using various two-dimensional NMR methods **(Supplementary Table 1)**. Statistical analysis of the spectral data by orthogonal projections to latent structures discriminant analysis (OPLS-DA) showed significant metabonomic differences between the erlotinib-resistant and sensitive cells **(Figures 1B and C)**. Changes in 14 metabolites mainly involved in glutathione, amino acids, nucleotides and choline metabolism **(Supplementary Figures 2A-C)** correlated with resistance in both cell line pairs **(Figure 1D & Supplementary Table 2)**. Noticeably, a significant drop in the intracellular levels of glutathione (GSH) accompanied erlotinib resistance **(Figure 1D & Supplementary Table 2)**. Such GSH decrease observed by NMR was independently confirmed using a colorimetric assay **(Figures 1E-F)**. This was intriguing, as drug resistance was traditionally associated with increased GSH levels [25, 26]. Nevertheless, GSH covalently binds some chemotherapeutic drugs leading to their glutathione-*S*-transferase-mediated extracellular export and resistance of cancer cells to these compounds [27, 28]. Hence, increased export of this metabolite in complex with erlotinib could account for the lower GSH levels in resistant cell lines. ^{1}H-NMR analysis of the culture medium from our four cell lines disproved this possibility by showing no difference in secreted GSH between TKI-resistant and sensitive cells **(Supplementary Figure 2D)**. Hence, decreased intracellular GSH levels in erlotinib-resistant cells are likely due to changes in GSH metabolism.

Erlotinib-resistant cells have lower expression of GSH synthesising enzymes

We investigated whether erlotinib-resistant cells differed from their sensitive counterparts in their GSH metabolic enzymes expression pattern. qPCR analysis revealed lower mRNA levels for GSH-synthesising enzymes (GCLC, GSS, GSR) in erlotinib-resistant cells compared to sensitive ones **(Figures 2A and B)**. In addition, mRNA levels for GCLM, the modulatory subunit of GCLC, were significantly lower in H1975 than in H3255 cells. In contrast, changes in the levels for GSH-

114 catabolic enzymes (GPX1/2/3, GGT and GSTpi/m1/zi) varied greatly between cell line pairs and
115 enzyme subtypes indicating no clear pattern (**Figure 2B**). Therefore, a reduction in GSH
116 biosynthesis becomes a sound explanation for the decreased GSH levels in EGFRm/T790M
117 erlotinib-resistant cells.

118 *Targeting GSH metabolism modulates the cellular response to erlotinib*

119 NMR results suggested that lower GSH levels associated with erlotinib resistance. To strengthen
120 this link, we employed siRNAs for GSH-metabolic enzymes to modulate GSH levels in our cell lines.
121 Silencing of GSH catabolic enzymes (GGT1, GPX1 and GSTpi) increased the response to erlotinib in
122 both the EGFRm PC9 and EGFRm/T790M PC9ER and H1975 cells (**Figure 2C and Supplementary**
123 **Figure 3C)**. This correlated with efficient targets' down-regulation and a corresponding increase in
124 GSH levels **(Supplementary Figures 3A and B)**. Conversely, silencing GSH-synthesising enzymes
125 (GCLC, GSS and GSR) lowered cellular GSH levels **(Supplementary Figures 3A and B)** and rendered
126 the sensitive PC9 cells erlotinib-resistant **(Figure 2C)**.

127 To validate our siRNA data, we used small-molecule inhibitors targeting the activity of
128 GSH pathway enzymes. Treatment with ethacrynic acid (EA), a known GST inhibitor, increased
129 GSH levels in erlotinib-resistant cells **(Figure 2D)** causing re-sensitisation of PC9ER and H1975 cells
130 to erlotinib **(Figures 2E-F)**. Similarly, GPXs inhibition using mercaptosuccinate (MS) increased
131 intracellular GSH levels **(Supplementary Figure 3D)** and the response of H1975 cells to erlotinib
132 **(Supplementary Figure 3E)**. Conversely, GCLC inhibition using buthionine sulphoximine (BSO) in
133 sensitive cells made them erlotinib-resistant **(Figures 2G and H)**, an effect associated with
134 decreased GSH levels **(Figure 2I)**. Furthermore, EA was also able to sensitize PC9ER cells to
135 gefitinib by increasing intracellular GSH (**Supplementary Figures 4A-C**). Taken together, these
136 data suggest that manipulating GSH levels controls the responsiveness of our cell lines to
137 erlotinib.

The NRF2 pathway controls GSH synthesis and responsiveness to erlotinib.

GCLC, GSS and GSR are transcriptional targets of NFE2-related factor 2 (NRF2)[29-31], a downstream target of EGFR[32]. We therefore hypothesised that NRF2 activity might be impaired in EGFRm/T790M cells. NRF2's transcriptional activity requires its nuclear localisation and NRF2 is also degraded through binding to KEAP1, a process counteracted by competitive interaction of the latter protein with PALB2 and/or SQSTM1 **(Figure 6F)**. Analysis of nucleo-cytoplasmic fractions and total lysates from our four cell lines revealed that NRF2 or KEAP1 localisation/expression had no differences between PC9 and PC9ER cells whereas H3255 cells showed higher nuclear NRF2 than H1975 cells **(Figure 3A, Supplementary Figure 5A)**. This correlated with increased KEAP1 expression in H1975 as compared to H3255 cells **(Figure 3A, Supplementary Figure 5B)**. Although these results alone may explain the difference in GSH pathway enzymes expression between the latter two cell lines, they cannot account for that seen between PC9 and PC9ER cells. However, SQSTM1 was down-regulated in both PC9ER and H1975 cells as compared to their erlotinib-sensitive counterparts **(Figure 3B**, quantified **Supplementary Figure 5C)** while PALB2 levels were lower in PC9ER as compared to PC9 cells **(Figure 3B**, quantified **Supplementary Figure 5D)**. Furthermore, NRF2 has been shown to be a transcriptional regulator of SQSTM1 and indeed, mRNA levels of SQSTM1 were found to be significantly lower in both the resistant cell-line pair **(Supplementary Figures 5E and F)**. Hence, inhibition of NRF2 activity through various mechanisms may be linked to erlotinib-resistance in NSCLC cells.

To test this hypothesis, we silenced NRF2, SQSTM1, PALB2 and KEAP1 in our cells. siRNA-mediated silencing of NRF2 **(Supplementary Figure 6A)** rendered PC9 cells erlotinib-resistant, a change associated with lower intracellular GSH **(Figures 3C and D)**. Indeed, NRF2-silenced cells showed down-regulation of the GSH-synthesising enzymes GCLC and GSR **(Supplementary Figure 6B)**, demonstrating a direct link between NRF2 activity and GSH synthesis. Similarly, SQSTM1 silencing **(Supplementary Figures 6C and D)** decreased the sensitivity of PC9 cells to erlotinib

(Figure 3E) in association with a drop in GSH levels **(Figure 3F)**. Conversely, KEAP1 down-regulation **(Supplementary Figure 6E)** sensitised EGFRm/T790M PC9ER cells to erlotinib **(Figure 3G)**, accompanied by increased GSH levels **(Figure 3H)** and increased transcription of GSH-synthesizing enzymes GCLC, GSR and GSS **(Supplementary Figure 6F)**. Finally, despite the changes in PALB2 between PC9ER and PC9 cells **(Figure 3B)**, silencing this protein in PC9 cells failed to induce erlotinib resistance or alter GSH levels **(Supplementary Figures 7A and B)**. Hence, modulation of NRF2 activity through KEAP1 and SQSTM1 regulates the sensitivity of NSCLC cells to erlotinib.

Inhibition of NRF2 activity and decreased GSH levels are direct consequences of the T790M mutation

Although lower GSH levels and NRF2 activity were associated with T790M-driven erlotinib resistance in our cell lines, this may still be incidental unless the T790M mutation directly induces these changes. We further expressed the active (L858R) or active/resistant (L858R/T790M) EGFR mutants in HEK293 cells that contain low endogenous EGFR levels **(Figure 4A)**. Unlike expression of the L858R-EGFR, expression of the L858R/T790M double-mutant receptor reduced intracellular GSH levels **(Figure 4B)**. This was associated with reduced PALB2 and SQSTM1 expression **(Figure 4C)**. Conversely, transfection with two independent siRNA sequences previously shown to selectively target T790M-mutant EGFR[33] sensitised PC9ER cells to erlotinib **(Supplementary Figures 7C and D)** and increased GSH levels **(Figures 4D and E)**. The latter correlated with a reversal of changes in the expression pattern of GSH metabolic enzymes observed between PC9 and PC9ER cells **(Figure 4F vs Figure 2B)** and with increased PALB2, SQSTM1 and NRF2 levels in T790M-silenced cells **(Figure 4G)**. Therefore, lower GSH levels in T790M NSCLC cells are a direct consequence of acquiring this mutation and the accompanying impairment of NRF2 activity.

Decrease in GSH correlates with increased nitric oxide levels

Since GSH buffers reactive oxidative species (ROS), we investigated whether lower GSH levels in erlotinib-resistant cells associated with elevated ROS. We performed flow cytometry analysis in the presence of dihydroethidine (DHE) and 4-amino-5-methylamino-2',7'-difluorofluorescein diacetate (DAF-FM) to detect superoxide and nitric oxide species, respectively. Erlotinib-resistant cells showed an increase in nitric oxide (NO) species **(Figure 5A)** although they did not show increased superoxide levels. To assess whether this could influence erlotinib resistance, we first silenced the expression of the three NO synthases, NOS1-3. While siRNA-mediated down-regulation of NOS2 and 3 did not impact on erlotinib resistance (not shown), NOS1 silencing sensitised PC9ER cells to erlotinib **(Figure 5B)**. Next, we quenched cellular NO in erlotinib-resistant cells with the NO-trap Carboxy-PTIO and revealed that this partially re-sensitised PC9ER cells to erlotinib **(Figure 5C)**. While these data suggest a role for NO in erlotinib resistance, the levels of changes observed as compared to those seen earlier **(Figures 2 and 3)** suggest that changes in NO are not solely responsible for resistance downstream of decreased GSH levels.

Ethacrynic acid administration re-sensitises EGFRm/T790M tumors to erlotinib in mouse xenografts.

The GST inhibitor EA restored GSH levels and erlotinib-sensitivity in EGFRm/T790M cells *in vitro* **(Figure 2)**. EA is still used as a diuretic in humans for conditions including high blood pressure and heart failure [34]. Hence, we hypothesised that co-administration of physiologically-relevant doses of EA might improve the responsiveness of EGFRm/T790M tumors to erlotinib *in vivo*. PC9 or PC9ER cells were injected subcutaneously in *nude* mice and tumours left to grow to 100 mm^3. The animals were then treated daily with erlotinib and EA alone or in combination. Co-administration of the drugs greatly inhibited tumour growth with 60% of the animals showing tumour volumes $\leq$300 mm^3 at 25 days while those treated with either drug alone showed more extensive disease **(Figure 6A)**. This was associated with increased survival **(Figure 6B)** and intra-tumoural GSH levels in combination-treated animals **(Figure 6C)**. EA did not have any effect on Erlotinib sensitivity of

PC9 xenografts in agreement with the lack of further added sensitisation to erlotinib obtained with this inhibitor *in vitro* **(Supplementary Figure 7E)**. Thus, co-administration of EA is probably a viable strategy for the management of erlotinib-resistant cancers in humans.

Decreased GSH synthetic enzymes expression characterises erlotinib-resistant patients

Finally, we assessed whether the decrease in GSH-synthetising enzymes observed in EGFRm/T790M cell lines *in vitro* also occurred in patients. First, we performed qPCR for GSS, GSR, GCLC and GCLM in paired biopsy samples from two patients prior to (EGFRm alone) and after acquiring EGFRm/T790M-mediated erlotinib resistance. In both cases, resistance was accompanied by a decrease in one or both of the rate-limiting enzymes for GSH biosynthesis, GCLC and GSS **(Figure 6D)**. Moreover, this association was not limited to syngeneic samples, as RNA-Seq of four pairs of unrelated patients' biopsies revealed lower expression of at least one of these enzymes in T790M tumours as compared to non-T790M samples **(Figure 6E)**. Therefore, decreased expression of GSH synthetic enzymes is probably associated with T790M-mediated erlotinib resistance in lung cancer patients.

DISCUSSION

EGFR TKIs such as erlotinib offer therapeutic benefit to NSCLC patients harbouring EGFRm [1-3]. However, the rapid development of resistance due in 50% of cases to acquisition of the secondary T790M EGFR mutation greatly limits the ability of these agents to prolong patient survival [5-8]. While decreased affinity of the EGFRm/T790M for erlotinib was thought responsible and new irreversible inhibitors may be promising in circumventing this, additional mechanisms of resistance are likely to be present. Indeed, EGFRm/T790M cells still demonstrate significant loss of sensitivity to an irreversible compound **(Supplementary Figure 1C)**. This suggested that resistance to erlotinib in EGFRm/T790M NSCLC cells is mediated through additional mechanisms.

Accumulating evidence suggests EGFR mutations to drive alteration in metabolic signatures, however, majority of them fail to demonstrate efficacy of targeting these molecules in clinical settings or *in vivo* models [35-37]. To identify novel resistance pathways, we performed ^{1}H-NMR metabonomic analysis of two independent NSCLC erlotinib-sensitive/resistant cell line pairs (PC9/PC9ER and H3255/H1975 cell lines). These were chosen according to several criteria. First, both resistant cell lines shared the same T790M resistance mutation. Second, while PC9ER cells were obtained through selecting PC9 cells with erlotinib making these two lines relatively isogenic, H3255 and H1975 cells are genetically unrelated. Third, the primary EGFR activating mutations in the two cell line pairs were different (ΔE746-A750 for PC9/PC9ER cells, L858R for H3255/H1975 cells). These criteria maximised the opportunity for metabolic changes shared by both cell line pairs to be solely dependent on the T790M mutation. One of the most striking differences highlighted by our analysis was a decrease in GSH levels in erlotinib-resistant cells **(Figures 1A-F)**. The GSH pathway has long been involved in cancer drug resistance [27, 28]. However, this was traditionally associated with increased GSH levels [25, 26]. Indeed, GSH covalently binds to some drug molecules in a GST-dependent manner leading to their cellular export and quenches ROS often requiring for these compounds to act [27, 28]. Therefore, an association between decreased GSH levels and EGFR-TKI resistance was surprising and warranted further investigation of its relevance to erlotinib responses.

Our experiments demonstrated that inhibition of GSH biosynthesis by either RNAi or small-molecules made erlotinib-sensitive cells resistant to the drug **(Figures 2C, G-I)**. Conversely, inhibition of GSH-degradation re-sensitised resistant cells to erlotinib **(Figures 2D-F)**. Hence, changes in GSH levels alone can modulate the response of NSCLC cells to this drug and decreased GSH levels accounts for erlotinib-resistance in PC9ER and H1975 cells. Comparative analysis revealed a transcriptional down-regulation of GSH-synthesising enzymes in T790M cells **(Figure 2B)** due to the impairment of NRF2, a downstream mediator of EGFR responsible for transcription of these enzymes **(Figures 3A and B)**. This occurred via upregulation of the NRF2 inhibitor KEAP1

and/or downregulation of PALB2 and SQSTM1, two proteins involved NRF2 stabilisation. Indeed, siRNA-mediated silencing of KEAP1 in T790M cells sensitised them to erlotinib **(Figures 3G and H)** while that of SQSTM1 or NRF2 made sensitive cells resistant to this drug **(Figures 3C-F)**. Importantly, decreased NRF2 activity and GSH levels in resistant cells were a direct consequence of acquiring the T790M mutation as introducing EGFRm/T790M in HEK293 cells, rather than EGFRm alone, reproduced the changes associated with erlotinib resistance **(Figures 4A-C)**. Conversely, silencing EGFRm/T790M in PC9ER cells reverted the changes in GSH levels and metabolic enzymes seen upon acquisition of resistance by PC9 cells **(Figures 4D-G)**.

It is unclear by what mechanism(s) the T790M mutation induces the observed transcriptional changes as the higher kinase activity of EGFRm/T790M [9] should further enhance NRF2 activity. However, mutant EGFRs differ from their wild-type counterparts in their sub-cellular localisation [38] which probably results in the EGFRm/T790M having different signalling partners as EGFRm or wild-type EGFR. Further research will be required to investigate this possibility.

We next attempted to identify the mechanism by which decreased GSH levels cause erlotinib resistance. GSH is a major cellular antioxidant [39], and its reduced expression could result in increased ROS. In addition, single nucleotide polymorphisms (SNPs) in anti-oxidant genes have been demonstrated to be associated with survival outcome in patients receiving TKI therapy [40]. While superoxide levels were unchanged, NO levels were raised in PC9ER as compared to PC9 cells **(Figure 5A)** and NOS1 silencing or NO quenching sensitised PC9ER cells to erlotinib **(Figures 5B and C)**. GSH is known to neutralise NO and protect against protein nitrosylation [41, 42]. It is worth noting that EGFR is a target of *S*-nitrosylation [43] but the consequence of this on erlotinib response is currently unknown. However, while our data suggest that NO probably contributes to erlotinib resistance, this does not fully explain the effects of reduced GSH. Glutathionylation plays a role in disease state by modifying the function of target proteins [44] and assessing changes to the

glutathionylation profile may identify proteins involved in EGFRm/T790M-mediated erlotinib resistance.

Regardless of the mechanism underlying erlotinib resistance downstream of decreased GSH levels, we showed that the GSH pathway could be manipulated for therapeutic benefit. Indeed, systemic administration of clinically-relevant doses of EA, a GST inhibitor [45], increased the intra-tumoural GSH levels **(Figure 6C)** and re-sensitised EGFRm/T790M tumours to erlotinib in a cancer cell xenograft mice model **(Figures 6A-C)**. Since EA is an orally available diuretic used in humans with limited toxicity [34], our findings could rapidly translate into clinical practice if this sensitisation also occurs in humans. Moreover, EA has already been used together with classical chemotherapeutics such as alkylating agents to prevent their GST-mediated cellular export [34], leading to improved clinical outcome. Therefore, EA may help manage erlotinib resistance in EGFRm-NSCLC patients and improve response to follow-on chemotherapeutic regimen. However, it is unclear whether decreased GSH levels only occurs downstream of the EGFRm/T790M or if this is a common feature of other erlotinib-resistance pathways such as c-Met amplification. Answering this prior to clinical exploitation of our findings will help more accurate patient selection for EA/erlotinib combined trials.

Finally, we show our findings to be clinically relevant using EGFRm and EGFRm/T790M lung cancer samples **(Figures 6D and E)**. The reduced number of samples analysed reflects the fact that repeated biopsy in NSCLC following the onset of EGFR TKI-resistance is rare although this practice is now changing. Nevertheless, we demonstrate in both syngenic and unrelated patient samples that mRNA levels for GSH synthesising enzymes are decreased in T790M tumours. Hence, probing for glutathione synthesizing enzymes may help, in a recurrent setting, to predict the response to combinatorial therapies of erlotinib and glutathione level increasing agents.

To sum up, we demonstrate that decreased intracellular level of GSH could mediate T790M-driven erlotinib resistance in NSCLC and highlight the molecular events involved **(Figure 6F)**.

311 Therapeutic strategies that increase intra-tumoural GSH levels may revert erlotinib resistance in
312 the clinic.

313

314 **MATERIALS AND METHODS**

315 **Materials:** Mercaptosuccinic acid (used at 50 μM), buthionine sulfoximine (used at 40 μM),
316 ethacrynic acid (used at 50 and 100μM in PC9 and H1975 cells, respectively) were purchased from
317 Sigma whereas EGFR Inhibitor 324674 was from Santa Cruz and Merck, respectively. Antibodies
318 against GSTpi, GPX1, GSS, GSR, GCLc, GSTpi, SQSTM1 and DPP3 were from Abcam; antibodies
319 targeting NRF2 and KEAP1 were from Santa Cruz and anti-PALB2 was from Novus. The specificity
320 of all antibodies employed here was assessed by disappearance of the respective signal following
321 selective targeting of the expression of the corresponding protein by siRNA treatment. Quantitect
322 primers targeting GSTpi, GPX1, GPX1, GSS, GSR, GCLc were from Qiagen. All other primers were
323 synthesised by Sigma. SiRNAs were purchased from Dharmacon. DHE was from Invitrogen and
324 DAF-FM from Sigma.

325 **Cell culture:** All cell lines were obtained from the CRUK cell line bank where they were
326 authenticated and mycoplasma status assessed through regular testing in our lab. Cell lines were
327 grown in RPMI with 10% fetal bovine serum at 37 °C, 5% CO_2.

328 **Extraction of the intracellular metabolites:** Intracellular metabolites were extracted as reported
329 previously[46, 47] with some modifications. In brief, 10^7 cells/condition were trypsinised and washed
330 thrice in ice-cold PBS prior to metabolite extraction. Cell pellets were re-suspended in 0.6 ml cold
331 water/methanol (1:2) and subjected to 3 freeze-thaw cycles prior to sonication in a wet ice bath
332 for 15 min (cycles: 1 min pulse followed by 1 min pause). Samples were then centrifuged (3200
333 *g*/4 ^{o}C, 10 min) and supernatants transferred into cold Eppendorfs. The remaining pellets were
334 extracted twice more by the same method. Supernatants from the 3 subsequent extractions were

335 combined, centrifuged (12000 *g*/4 ^{o}C, 10 min) and freeze-dried following vacuum-driven
336 methanol evaporation. Lyophilized samples were stored at -80 ^{o}C. Ten biological replicates were
337 used for each group of cells.

338 **Cellular metabonomic analysis by ^{1}H-NMR:** Freeze-dried intracellular metabolites extracts were
339 dissolved in 600 µL phosphate buffer 0.1 M (pH 7.4, 99.9% D2O) containing 0.001% sodium 3-
340 trimethylsilyl-1-[2,2,3,3-^{2}H4] propionate (TSP) as previously described[48]. All samples were
341 centrifuged (12000 *g*/4 ^{o}C, 10 min) after short vortexing and supernatants transferred into the 5
342 mm NMR tubes for NMR detection. All 1D ^{1}H-NMR spectra were acquired on a Bruker AVIII 600
343 MHz NMR spectrometer equipped with a cryogenic probe (BrukerBiospin, Germany) at 298 K. The
344 first increment of NOESY pulse sequence was employed with continuous wave irradiation on the
345 water peak during recycle delay and mixing time for water suppression. Recycle delay of 2 s and
346 mixing time of 100 ms were set. The 90° pulse was adjusted to 10 µs approximately and 64 scans
347 were collected into 32k data points with the spectral width of 20 ppm. For metabolite
348 assignments, 2D-NMR spectra including ^{1}H–^{1}H COSY, ^{1}H–^{1}H TOCSY, ^{1}H *J*-resolved, ^{1}H–^{13}C HSQC and
349 ^{1}H-^{13}C HMBC for typical samples were acquired and processed as described previously[49] .

350 **NMR data analysis:** The spectral region at δ0.5-9.5 was integrated into bins with the width of
351 0.002 ppm using AMIX package (v3.8, Bruker Biospin). The range (δ4.7-5.2) was removed to
352 eliminate the effects of water peak suppression. Each bin area was normalized to the total area of
353 the respective spectrum. Multivariate data analysis was performed with the software SIMCA-P+ (v
354 12.0, Umetrics, Sweden). The model was built using the orthogonal projection to latent structure-
355 discriminant analysis (OPLS-DA) [50] with Pareto variance (Par) scaling and 7-fold cross validation.
356 The parameter $R^{2}X$ was the variation of X explained by the model and Q^{2} represented the
357 predictability of the model. The validation of all the models was further ensured by CV-ANOVA (*p*
358 < 0.05)[51]. To assist the biological interpretation of the loadings generated from the models, the
359 loadings was firstly back-transformed [52] and then plotted with color-coded OPLS-DA coefficients in

MATLAB 7.1 using an in-house script[53]. The color code corresponded to the absolute value of the OPLS-DA coefficients ($|r|$), indicating the contribution of each variable to explain the intergroup differentiation. The value of $|r|$, greater than 0.602, was considered to be significant ($n = 10$, $p < 0.05$).

Glutathione colorimetric assay: A GSH colorimetric assay kit was purchased from BioAssay Systems and used according to the manufacturer's instructions.

siRNA transfection: $1x10^4$ PC9, PC9ER or H1975 cells per well in 6 well-plates were transfected with siRNAs at 25 nM (Dharmacon) for 24 h using RNAiMax (Invitrogen) following the manufacturer's protocol. Each protein was targeted with a mix of 4 sequences. $4x10^3$ cells were re-seeded and then incubated at 37 °C/5% CO_2 for 24 h for target silencing prior to further experiment steps.

Cell survival assay: For ethacrynic acid , buthionine sulfoximine and mercaptosuccinic acid, cells were pre-treated for 4 h prior to erlotinib addition (100 nM) for 48 h. Cells were then fixed and stained for 20 min with a 25% methanol/0.5% crystal violet solution. Plates were washed in running water, air-dried and the stain dissolved in 10% acetic acid on a shaker prior to absorbance at 595 nm.

Quantitative PCR: Total cellular mRNA was extracted using the RNeasy kit (Qiagen) and converted to cDNA with a High Capacity cDNA Reverse Transcription Kit (Applied Biosystems). mRNA levels were quantified using a Fast SYBR Green Master Mix (Applied Biosystems) on a 7900HT Fast Real time PCR System (Applied Biosystems). qBase software was used for data analysis using TATA-binding protein and β-Actin as internal controls. The primers used were listed below (F, forward; R, reverse): GCLm: (F): GGCACAGGTAAAACCAAATAGTAAC, (R):CAAATTGTTTAGCAAATGCAGTCA; GPX2: (F): TAAGTGGGCTCAGGCCTCTCT, (R): GGTCATAGAAGGACTTGGCAATG; GPX3: (F): GACAAGAGAAGTCGAAGATG, (R): CTTCCTGTAGTGCATTCAGTT; GSTz1: (F):

TCCTATTTCCGAAGCTCCTGC, (R): TTCAGTGCCTGGAAGTCCTTAG; GSTm1: (F): CTATGATGTCCTTGACCTCCACCGTATA, (R): ATGTTCACGAAGGATAGTGGGTAGCTGA; Beta-Actin: (F): TCCTCCTGAGCGCAAGTACTC, (R): CTGCTTGCTGATCCACATCTG; KEAP1: (F): CAGATTGGCTGTGTGGAGTT, (R): GCTGTTCGCAGTCGTACTTG; SQSTM1: (F): CTGGGACTGAGAAGGCTCAC, (R): GCAGCTGATGGTTTGGAAAT; TBP: (F): TGCACAGGAGCCAAGAGTGAA, (R): CACATCACAGCTCCCCACCA; NRF2 primers: (F): GAGAGCCCAGTCTTCATTGC, (R): TGCTCAATGTCCTGTTGCAT. Primers against the other targets were purchased from Qiagen: GCLc (QT00037310), GGT1 (QT00029470), GPX1 (QT00203392), GSTp1 (QT00086401), GSS (QT00014413), GSR (QT00038325).

Tissue mRNA extraction and qPCR: The origin of tissues and techniques used are as previously reported [54]. In short, samples were obtained from EGFR-mutant lung adenocarcinoma patients with acquired erlotinib resistance under Human Investigations Protocol #111000928 (Yale Cancer Center, New Haven, CT). Those were reviewed by a pathologist to ensure adequate tumor content. Tumor areas were circled and microdissection performed to enrich for tumor content.

Tissue mRNA extraction and RNA-Seq: The Illumina TruSeq RNA Sample Preparation Kit was used for RNA tissue extraction and analysis done as previously described [55].

Western blotting: Cells were lysed using 0.5% Triton X-100, 150 mM NaCl, 2 mM EDTA, 10% glycerol supplemented with protease inhibitors cocktail tablets (Roche Diagnostics), 10 mM β-glycerophosphate, 1 mM Na_3VO_4 and 10 mM NaF. Equal protein amounts were analysed by SDS-PAGE/Western blotting using the antibodies indicated.

Flow cytometry analysis of oxidative species: Cells ($15x10^4$/well in 6-well plate) were treated with 10 μM DAF-FM or DHE for 30 min, washed with PBS, trypsinised, pelleted and re-suspended in 1 ml of PBS prior to flow cytometry using a BD FACSCalibur. The geometric mean intensity was determined using FlowJo (Tree Star, Inc).

Animal experiments: $5x10^6$ PC9ER or PC9 cells were injected subcutaneously into the flank of female BALB/c nude mice and the tumors grew until they reached 100 mm^3. Mice were then randomized into 3 groups (n=10) and treated by intraperitoneal injection of 25 mg/kg/day Erlotinib/0.5% w/v methylcellulose and/or 6 mg/kg/day ethacrynic acid/1% Tween 80 in distilled water. Such treatments were administered daily from day 7 to 26. Tumors were measured by caliper and volumes calculated as $V = ½*L*W^2$ (L; length, W; width of tumor). Data analysis was performed by an investigator blinded to the experimental conditions. All experiments complied with ethical regulations as enforced by the local committee.

ACKNOWLEDGEMENTS

HRT/YLW acknowledge the financial supports from the Ministry of Science and Technology of China (2012CB934004), National Natural Science Foundation of China (81590953, 81590950, 91439102, 21375144). MJS/OP are funded by the European Commission's FP7 under the LungTarget consortium, the AICR and CTRT. Also, MJS is supported by CR-UK and UK Dept of Health/NIHR Imperial ECMC and BRC.

REFERENCES

1. Mok TS, Wu YL, Yu CJ *et al.* Randomized, placebo-controlled, phase II study of sequential erlotinib and chemotherapy as first-line treatment for advanced non-small-cell lung cancer. *J Clin Oncol* 2009; **27**:5080-5087.

2. Lynch TJ, Bell DW, Sordella R *et al.* Activating mutations in the epidermal growth factor receptor underlying responsiveness of non-small-cell lung cancer to gefitinib. *N Engl J Med* 2004; **350**:2129-2139.

3. Paez JG, Janne PA, Lee JC *et al.* EGFR mutations in lung cancer: correlation with clinical response to gefitinib therapy. *Science* 2004; **304**:1497-1500.

4. Stewart EL, Tan SZ, Liu G, Tsao MS. Known and putative mechanisms of resistance to EGFR targeted therapies in NSCLC patients with EGFR mutations-a review. *Transl Lung Cancer Res* 2015; **4**:67-81.

5. Kosaka T, Yatabe Y, Endoh H *et al.* Analysis of epidermal growth factor receptor gene mutation in patients with non-small cell lung cancer and acquired resistance to gefitinib. *Clin Cancer Res* 2006; **12**:5764-5769.

6. Balak MN, Gong Y, Riely GJ *et al.* Novel D761Y and common secondary T790M mutations in epidermal growth factor receptor-mutant lung adenocarcinomas with acquired resistance to kinase inhibitors. *Clin Cancer Res* 2006; **12**:6494-6501.

7. Kobayashi S, Boggon TJ, Dayaram T *et al.* EGFR mutation and resistance of non-small-cell lung cancer to gefitinib. *N Engl J Med* 2005; **352**:786-792.

8. Pao W, Miller VA, Politi KA *et al.* Acquired resistance of lung adenocarcinomas to gefitinib or erlotinib is associated with a second mutation in the EGFR kinase domain. *PLoS Med* 2005; **2**:e73.

9. Yoshikawa S, Kukimoto-Niino M, Parker L *et al.* Structural basis for the altered drug sensitivities of non-small cell lung cancer-associated mutants of human epidermal growth factor receptor. *Oncogene* 2012.

10. Cross DA, Ashton SE, Ghiorghiu S *et al.* AZD9291, an irreversible EGFR TKI, overcomes T790M-mediated resistance to EGFR inhibitors in lung cancer. *Cancer Discov* 2014; **4**:1046-1061.

11. Walter AO, Sjin RT, Haringsma HJ *et al.* Discovery of a mutant-selective covalent inhibitor of EGFR that overcomes T790M-mediated resistance in NSCLC. *Cancer Discov* 2013; **3**:1404-1415.

12. Zhang Q, Liu Y, Gao F *et al.* Discovery of EGFR selective 4,6-disubstituted pyrimidines from a combinatorial kinase-directed heterocycle library. *J Am Chem Soc* 2006; **128**:2182-2183.

13. Miller VA, Hirsh V, Cadranel J *et al.* Afatinib versus placebo for patients with advanced, metastatic non-small-cell lung cancer after failure of erlotinib, gefitinib, or both, and one or two lines of chemotherapy (LUX-Lung 1): a phase 2b/3 randomised trial. *Lancet Oncol* 2012.

14. Costa DB, Kobayashi SS. Whacking a mole-cule: clinical activity and mechanisms of resistance to third generation EGFR inhibitors in EGFR mutated lung cancers with EGFR-T790M. *Transl Lung Cancer Res* 2015; **4**:809-815.

15. Jones RG, Thompson CB. Tumor suppressors and cell metabolism: a recipe for cancer growth. *Genes Dev* 2009; **23**:537-548.

16. Cavill R, Kamburov A, Ellis JK *et al.* Consensus-Phenotype Integration of Transcriptomic and Metabolomic Data Implies a Role for Metabolism in the Chemosensitivity of Tumour Cells. *Plos Computational Biology* 2011; **7**.

17. Jang M, Kim SS, Lee J. Cancer cell metabolism: implications for therapeutic targets. *Exp Mol Med* 2013; **45**:e45.

18. Zhao Y, Butler EB, Tan M. Targeting cellular metabolism to improve cancer therapeutics. *Cell Death Dis* 2013; **4**:e532.

19. Sreekumar A, Poisson LM, Rajendiran TM *et al.* Metabolomic profiles delineate potential role for sarcosine in prostate cancer progression. *Nature* 2009; **457**:910-914.

20. Boros LG, Cascante M, Lee WN. Metabolic profiling of cell growth and death in cancer: applications in drug discovery. *Drug Discov Today* 2002; **7**:364-372.

21. Wang YH, Zhang LM, Chen WL *et al.* Rapid Diagnosis and Prognosis of de novo Acute Myeloid Leukemia by Serum Metabonomic Analysis. *Journal of Proteome Research* 2013; **12**:4393-4401.

22. Serkova NJ, Spratlin JL, Eckhardt SG. NMR-based metabolomics: translational application and treatment of cancer. *Curr Opin Mol Ther* 2007; **9**:572-585.

23. Tian Y, Nie X, Xu S *et al.* Integrative metabonomics as potential method for diagnosis of thyroid malignancy. *Scientific Reports* 2015; **5**.

24. Alama A, Orengo AM, Ferrini S, Gangemi R. Targeting cancer-initiating cell drug-resistance: a roadmap to a new-generation of cancer therapies? *Drug Discov Today* 2012; **17**:435-442.

480 25. Brozovic A, Ambriovic-Ristov A, Osmak M. The relationship between cisplatin-induced reactive
481 oxygen species, glutathione, and BCL-2 and resistance to cisplatin. *Crit Rev Toxicol* 2010; **40**:347-
482 359.
483 26. Bracht K, Boubakari, Grunert R, Bednarski PJ. Correlations between the activities of 19 anti-
484 tumor agents and the intracellular glutathione concentrations in a panel of 14 human cancer cell
485 lines: comparisons with the National Cancer Institute data. *Anticancer Drugs* 2006; **17**:41-51.
486 27. Provost K, Bouvet-Muller D, Crauste-Manciet S *et al.* EXAFS structural study of platinum-based
487 anticancer drugs degradation in presence of sulfur nucleophilic species. *Biochimie* 2009; **91**:1301-
488 1306.
489 28. Rappa G, Lorico A, Flavell RA, Sartorelli AC. Evidence that the multidrug resistance protein
490 (MRP) functions as a co-transporter of glutathione and natural product toxins. *Cancer Res* 1997;
491 **57**:5232-5237.
492 29. Bell KF, Fowler JH, Al-Mubarak B, Horsburgh K, Hardingham GE. Activation of Nrf2-regulated
493 glutathione pathway genes by ischemic preconditioning. *Oxid Med Cell Longev* 2011;
494 **2011**:689524.
495 30. Kato K, Takahashi K, Monzen S *et al.* Relationship between radiosensitivity and Nrf2 target
496 gene expression in human hematopoietic stem cells. *Radiat Res* 2010; **174**:177-184.
497 31. Sekhar KR, Crooks PA, Sonar VN *et al.* NADPH oxidase activity is essential for Keap1/Nrf2-
498 mediated induction of GCLC in response to 2-indol-3-yl-methylenequinuclidin-3-ols. *Cancer Res*
499 2003; **63**:5636-5645.
500 32. Papaiahgari S, Zhang Q, Kleeberger SR, Cho HY, Reddy SP. Hyperoxia stimulates an Nrf2-ARE
501 transcriptional response via ROS-EGFR-PI3K-Akt/ERK MAP kinase signaling in pulmonary epithelial
502 cells. *Antioxid Redox Signal* 2006; **8**:43-52.
503 33. Chen G, Kronenberger P, Teugels E, Umelo IA, De Greve J. Effect of siRNAs targeting the EGFR
504 T790M mutation in a non-small cell lung cancer cell line resistant to EGFR tyrosine kinase

505 inhibitors and combination with various agents. *Biochem Biophys Res Commun* 2013; **431**:623-
506 629.
507 34. Somberg JC, Molnar J. The pleiotropic effects of ethacrynic acid. *Am J Ther* 2009; **16**:102-104.
508 35. Makinoshima H, Takita M, Saruwatari K *et al.* Signaling through the Phosphatidylinositol 3-
509 Kinase (PI3K)/Mammalian Target of Rapamycin (mTOR) Axis Is Responsible for Aerobic Glycolysis
510 mediated by Glucose Transporter in Epidermal Growth Factor Receptor (EGFR)-mutated Lung
511 Adenocarcinoma. *J Biol Chem* 2015; **290**:17495-17504.
512 36. Serizawa M, Kusuhara M, Zangiacomi V *et al.* Identification of metabolic signatures associated
513 with erlotinib resistance of non-small cell lung cancer cells. *Anticancer Res* 2014; **34**:2779-2787.
514 37. Xie C, Jin J, Bao X *et al.* Inhibition of mitochondrial glutaminase activity reverses acquired
515 erlotinib resistance in non-small cell lung cancer. *Oncotarget* 2016; **7**:610-621.
516 38. Chung BM, Raja SM, Clubb RJ *et al.* Aberrant trafficking of NSCLC-associated EGFR mutants
517 through the endocytic recycling pathway promotes interaction with Src. *BMC Cell Biol* 2009;
518 **10**:84.
519 39. Schafer FQ, Buettner GR. Redox environment of the cell as viewed through the redox state of
520 the glutathione disulfide/glutathione couple. *Free Radic Biol Med* 2001; **30**:1191-1212.
521 40. Xu Y, Pan Q, Wang C *et al.* Genetic polymorphisms in oxidative stress-related genes are
522 associated with clinical outcome in patients with advanced non-small cell lung cancer receiving
523 tyrosine kinase inhibitors. *Am J Cancer Res* 2014; **4**:934-942.
524 41. Pedersen JZ, De Maria F, Turella P *et al.* Glutathione transferases sequester toxic dinitrosyl-
525 iron complexes in cells. A protection mechanism against excess nitric oxide. *J Biol Chem* 2007;
526 **282**:6364-6371.
527 42. Aquilano K, Baldelli S, Ciriolo MR. Glutathione is a crucial guardian of protein integrity in the
528 brain upon nitric oxide imbalance. *Commun Integr Biol* 2011; **4**:477-479.
529 43. Switzer CH, Glynn SA, Cheng RY *et al.* S-nitrosylation of EGFR and Src activates an oncogenic
530 signaling network in human basal-like breast cancer. *Mol Cancer Res* 2012; **10**:1203-1215.

531 44. Ghezzi P. Protein glutathionylation in health and disease. *Biochim Biophys Acta* 2013;
532 **1830**:3165-3172.
533 45. Ploemen JH, van Ommen B, Bogaards JJ, van Bladeren PJ. Ethacrynic acid and its glutathione
534 conjugate as inhibitors of glutathione S-transferases. *Xenobiotica* 1993; **23**:913-923.
535 46. Li HD, Zhu WD, Zhang LK *et al.* The metabolic responses to hepatitis B virus infection shed new
536 light on pathogenesis and targets for treatment. *Scientific Reports* 2015; **5**.
537 47. Zhang LM, Wang LM, Hu YL *et al.* Selective metabolic effects of gold nanorods on normal and
538 cancer cells and their application in anticancer drug screening. *Biomaterials* 2013; **34**:7117-7126.
539 48. Jiang LM, Huang J, Wang YL, Tang HR. Eliminating the dication-induced intersample chemical-
540 shift variations for NMR-based biofluid metabonomic analysis. *Analyst* 2012; **137**:4209-4219.
541 49. An YP, Xu WX, Li HH *et al.* High-Fat Diet Induces Dynamic Metabolic Alterations in Multiple
542 Biological Matrices of Rats. *Journal of Proteome Research* 2013; **12**:3755-3768.
543 50. Trygg J, Wold S. Orthogonal projections to latent structures (O-PLS). *Journal of Chemometrics*
544 2002; **16**:119-128.
545 51. Eriksson L, Trygg J, Wold S. CV-ANOVA for significance testing of PLS and OPLS (R) models.
546 *Journal of Chemometrics* 2008; **22**:594-600.
547 52. Cloarec O, Dumas ME, Craig A *et al.* Statistical total correlation spectroscopy: an exploratory
548 approach for latent biomarker identification from metabolic 1H NMR data sets. *Anal Chem* 2005;
549 **77**:1282-1289.
550 53. Li D, Zhang LL, Dong FC *et al.* Metabonomic Changes Associated with Atherosclerosis
551 Progression for LDLR-/- Mice. *Journal of Proteome Research* 2015; **14**:2237-2254.
552 54. de Bruin EC, Cowell C, Warne PH *et al.* Reduced NF1 Expression Confers Resistance to EGFR
553 Inhibition in Lung Cancer. *Cancer Discov* 2014; **4**:606-619.
554 55. Huang S, Holzel M, Knijnenburg T *et al.* MED12 controls the response to multiple cancer drugs
555 through regulation of TGF-beta receptor signaling. *Cell* 2012; **151**:937-950.

556

557

558 **FIGURE LEGENDS**

559 **Figure 1:** (A) Typical 600 MHz ^{1}H-NMR spectra of aqueous extracts from PC9, PC9-ER, H3255 and
560 H1975 cells. The region (δ5.0-9.5) is vertically expanded four times (×4). Data representative of
561 n=10. Orthogonal projections to latent structures discriminant analysis (OPLS-DA) score plots (left)
562 and coefficient plots (right) for ^{1}H-NMR spectra of aqueous cellular extracts from PC9ER and PC9
563 showing significantly differentiated metabolites (B), H1975 and H3255 (C). Models validated by
564 CV-ANOVA, $p=2.36 \times 10^{-17}$ (B) and $p=3.04 \times 10^{-19}$ (C). The Q^2 is 0.99 for both models. The colour
565 scale for coefficient plots reflects the differences in the contribution of metabolite variations
566 between groups. $|r|$ cut-off value is 0.602 (n=10, p<0.05). For identification of peak numbers, see
567 Suppl. Table 1 and Fig 1D. (D) Metabolites showed statistically significant differences between
568 resistant and sensitive cells in both cell line pairs with statistically significant "decreases" or
569 "increases" detected in the erlotinib-resistant (ER) cells as compared to sensitive (ES) ones. (E-F)
570 GSH levels in PC9 and PC9ER (E) or H3255 and H1975 (F) cells determined by colorimetric assay.
571 Data are average ± SEM of n=4. Statistics: Student t-test. ***; p<0.001. See also Supp Figure 1.

572 **Figure 2:** Intracellular GSH levels modulate response to erlotinib. (A) Schematics of the GSH
573 metabolic pathway. White boxes; synthesising and grey boxes; catabolic enzymes. (B) RT-qPCR for
574 GSH pathway enzymes in PC9, PC9ER, H3255 and H1975 cells. Data are relative mRNAs levels in
575 PC9ER (upper panel) and H1975 (lower panel) normalised to those in PC9 and H3255 cells,
576 respectively. (C) PC9 and PC9ER cells were transfected with siRNA targeting GSH catabolic (grey
577 bars) and synthesising (white bars) enzymes or a non-targeting control (NT) and cell survival to
578 erlotinib (50nM) monitored by crystal violet staining. Data for the relative survival to erlotinib are
579 normalised to non-targeting control. (D-I) Survival to erlotinib of PC9ER (D) and H1975 (F) cells
580 treated with ethacrynic acid (EA) or PC9 (G) and H3255 (H) cells treated with
581 Buthioninesulphoximine (BSO) was monitored by crystal violet staining. Accompanying changes in
582 GSH levels in PC9ER (E) and PC9 (I) cells were assessed by colorimetric assay. (E, F, G, H) Data are

583 the relative responsiveness to erlotinib normalised to vehicle (-; DMSO). (B to I) Data
584 representative of ≥3 experiments and are average of n=3 ± SEM. Statistics; (E, F, G, H) ANOVA, (B,
585 C, D and I) Student *t*-test, *; $p \leq 0.05$, **; $p \leq 0.01$, ***; $p \leq 0.001$. See also Supp Figures 2-3.

586 **Figure 3:** Erlotinib-resistance correlates with decreased NRF2 activity. (A and B) Sub-cellular
587 fractions (A) and total lysates (B) from PC9, PC9ER, H3255 and H1975 cells were analysed by SDS-
588 PAGE/Western blotting for the indicated proteins. Detection of Lamin and Tubulin was used as
589 loading controls for nuclear fractions and total lysates or cytoplasmic fractions, respectively. (C-H)
590 PC9 cells transfected with non-targeting (NT), NRF2 or SQSTM1 siRNAs (C-F) or PC9ER cells
591 transfected with KEAP1 or NT siRNAs (H-K) were treated with erlotinib and survival assessed by
592 crystal violet staining (C, E, G). GSH levels were measured by colorimetric assay (D, F, H). (C-H)
593 Data are average of n=4 ± SEM. Statistics; Student *t*-test,*; $p \leq 0.05$, **; $p \leq 0.01$, ***; $p \leq 0.001$. See
594 also Supp Figures 4-5.

595 **Figure 4:** Expression of EGFRm/T790M decreases intracellular GSH levels and NRF2 activity. (A-D)
596 HEK293 cells were transfected with empty vector control (EV), activated L858R-EGFR or
597 activated/resistant L858R/T790M EGFR mutant constructs. (A) RT-qPCR for EGFR, (B) colorimetric
598 assay for GSH levels and (C) cell fractionation followed by SDS-PAGE/Western blotting for the
599 indicated proteins were done on stable cell lines. Detection of Lamin and Tubulin was used as
600 loading controls for nuclear and cytoplasmic fractions, respectively. (D-G) PC9ER cells transfected
601 with an EGFR T790M-specific or NT siRNAs were subjected to (D) treatment with erlotinib prior to
602 crystal violet staining, (E) colorimetric assay for intracellular GSH levels, (F) qPCR for GSH
603 metabolic enzymes or (G) SDS-PAGE/Western blotting. All data representative of ≥3 experiments.
604 (A, B, D, E, F) Values are average of n=4 ± SEM. Statistics; (A, B, D) ANOVA, (E and F) Student *t*-
605 test,*; $p \leq 0.05$, **; $p \leq 0.01$, ***; $p \leq 0.001$. See also Supp Figure 6.

606 **Figure 5:** Changes in NO levels modulate erlotinib response. (A) NO levels in PC9 and PC9ER cells
607 were compared by FACS using DAF-FM. Left; FACS profile, Right; fold changes in geometric mean.

608 (B) PC9ER cells transfected with non-targeting (NT) or NOS1 siRNAs or (C) PC9 and PC9ER cells
609 treated ± an NO-trap were exposed to a dose range of erlotinib. Cell survival was determined by
610 crystal violet staining. Statistics; Student *t*-test,*; $p \leq 0.05$.

611 **Figure 6:** Systemic EA administration re-sensitises PC9ER mouse xenografts to erlotinib. Nude
612 mice (n=10/condition) were injected subcutaneously with PC9ER cells and treatment started
613 when tumours reached 100 mm^3. (A) Tumour volume and (B) animals survival were monitored for
614 27 days. (A) Data are average ± SEM. (B) End-point events occur when tumour volumes ≥300
615 mm^3. Log-Rank test, $P_{ab}<0.01$, $P_{bc}<0.01$. (C) Following the last treatment, intratumoral GSH levels
616 were measured *ex vivo* by colorimetric assay. Statistics; (A) ANOVA, (C), Student *t*-test, *; $p< 0.05$;
617 **; $p< 0.01$. GSH synthesising enzymes expression is decreased in EGFRm/T790M patient
618 tumours. mRNA levels for the indicated enzymes were compared by qPCR in two patients before
619 (pre-T790M) and after (post-T790M) onset of T790M-mediated erlotinib resistance (D) or by RNA-
620 Seq in 4 pairs of unrelated patients with (Pt1-4) or without (Pt5-8) T790M (™) (E). Data in T790M
621 samples are normalised to those in the corresponding non-T790M samples. (F) Model of changes
622 occurring downstream of T790M-EGFR.

623

Figure 1

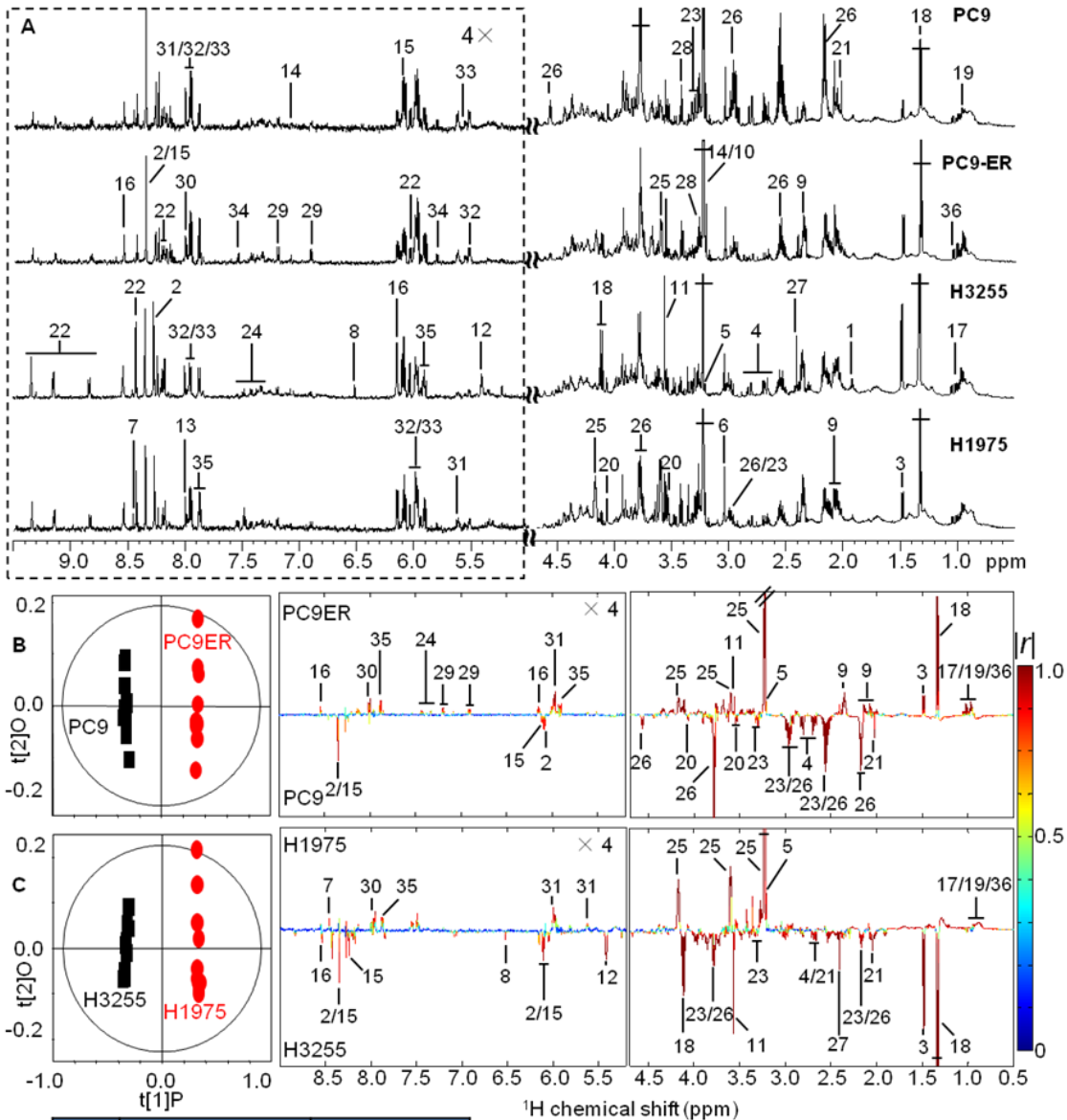

D

Key	Metabolite	ER/ES
2	Adenosine	Decrease
4	Aspartate	Decrease
5	Choline	Increase
15	Inosine	Decrease
17	Isoleucine	Increase
19	Leucine	Increase
21	*N*-acetyl aspartate	Decrease
23	**GSSG**	**Decrease**
25	Phosphocholine	Increase
26	**GSH**	**Decrease**
30	UDP	Increase
31	UDPG	Increase
35	Uridine	Increase
36	Valine	Increase

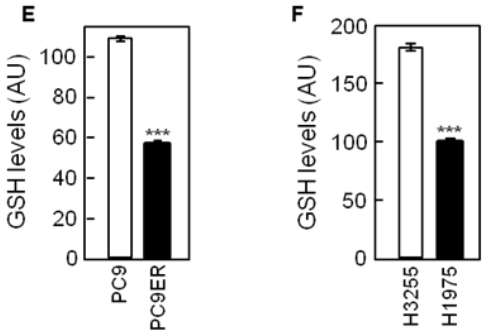

627 **Figure 2**

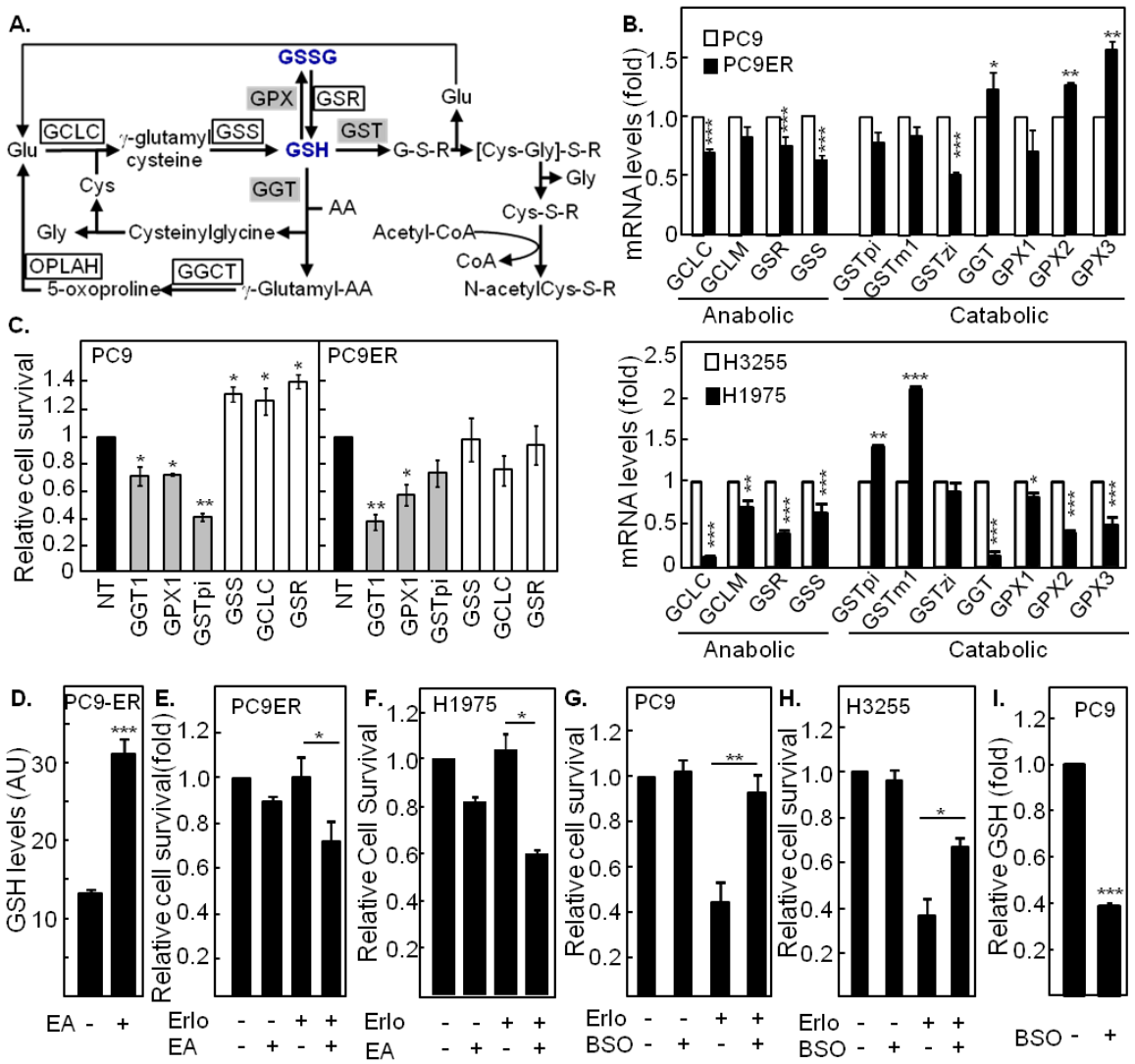

628

629

630 **Figure 3**

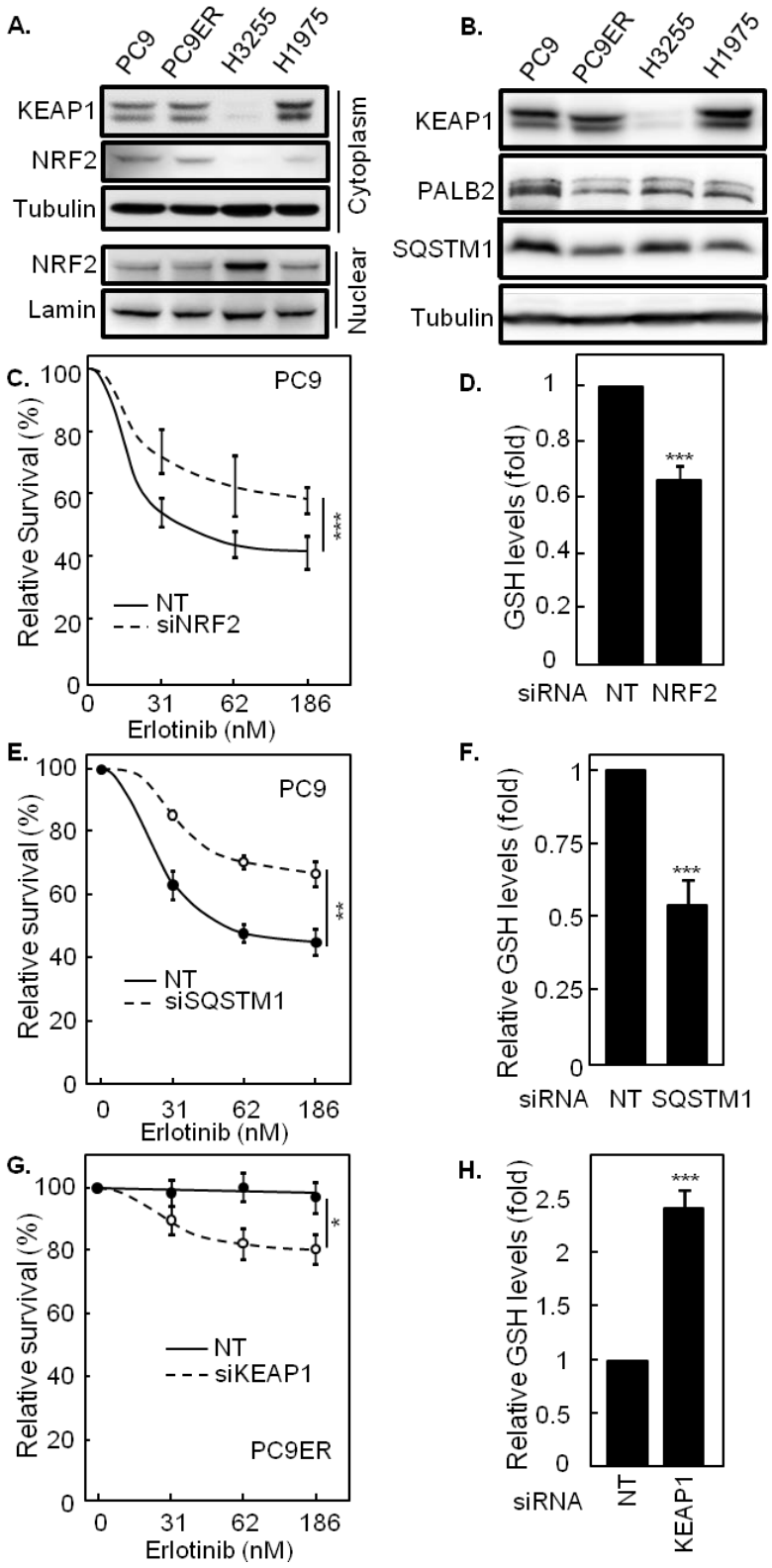

631

632

633 **Figure 4**

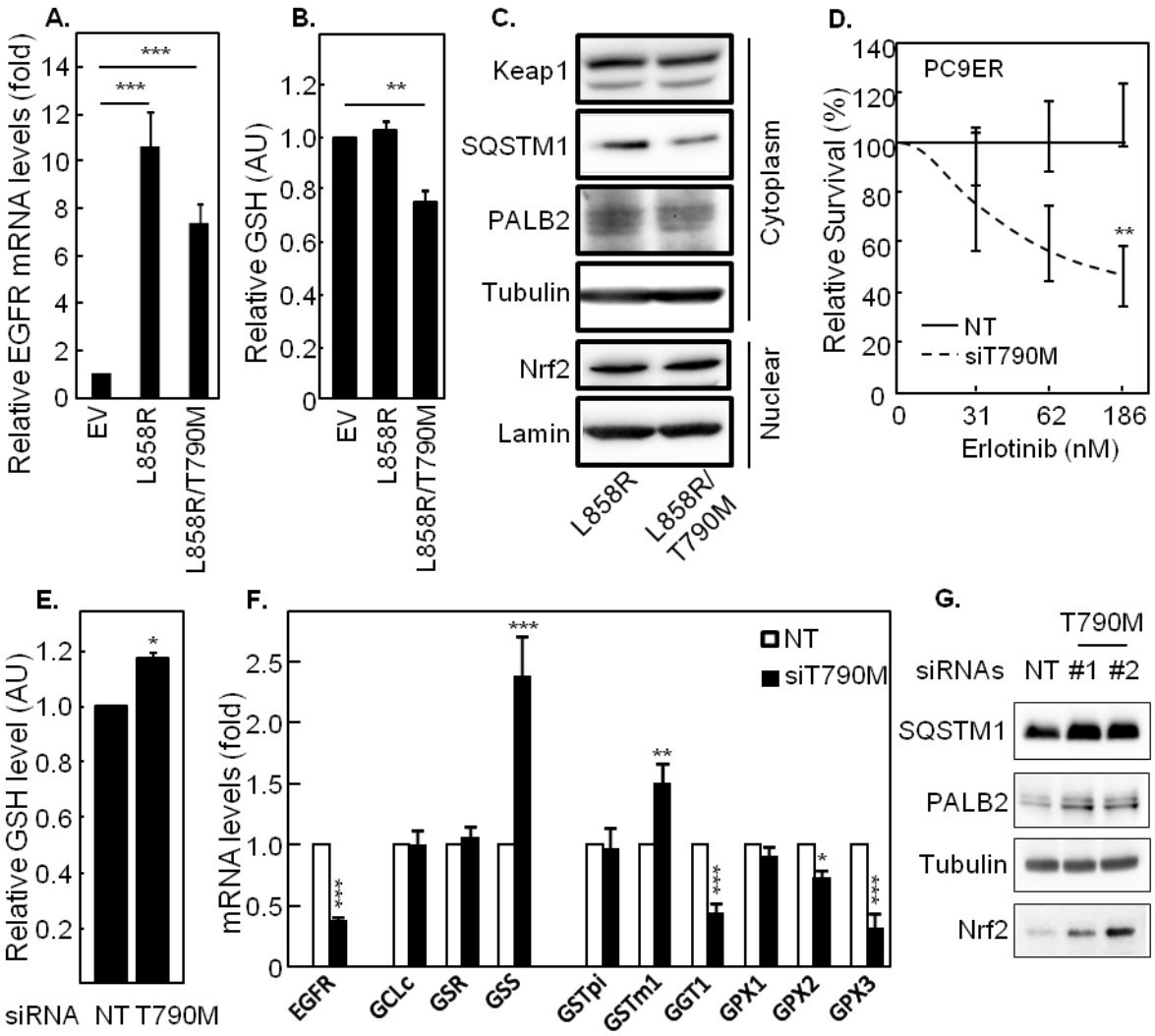

634

635

Figure 5

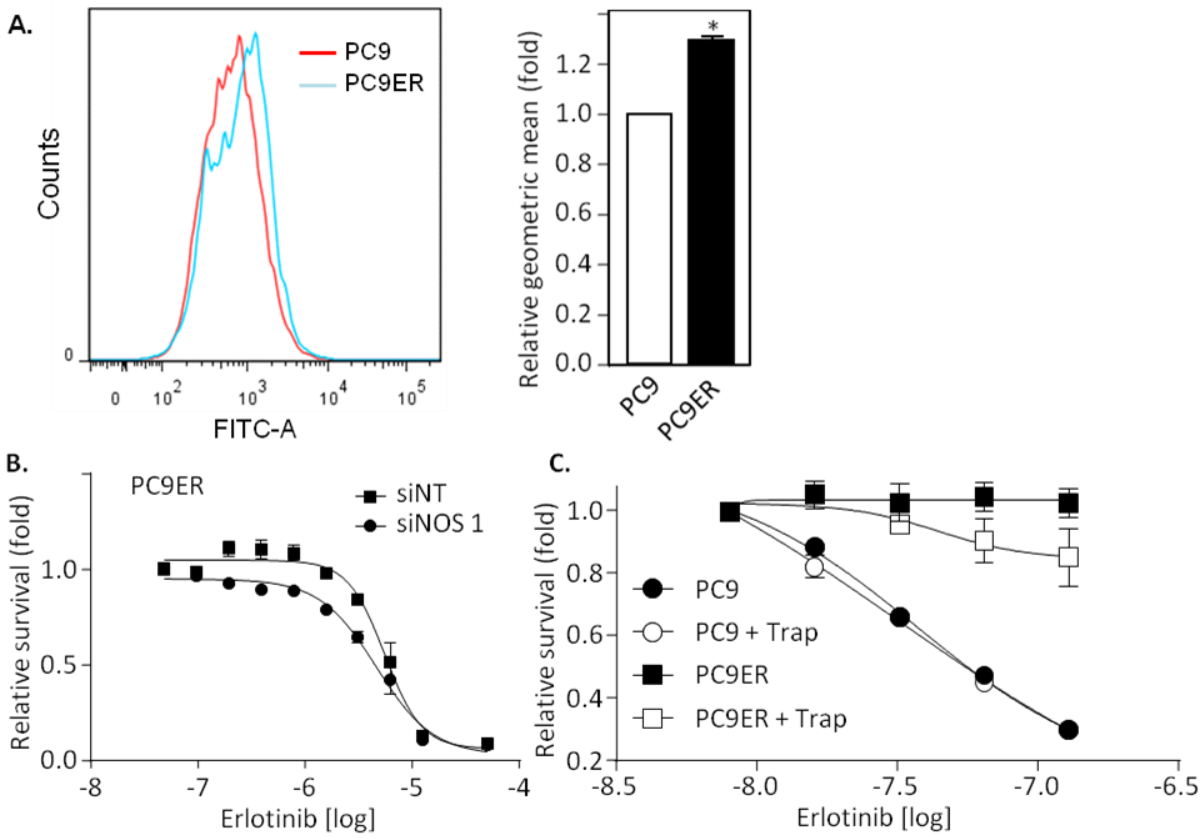
A.
PC9
PC9ER
Counts
FITC-A
Relative geometric mean (fold)
PC9
PC9ER
B.
PC9ER
siNT
siNOS 1
Relative survival (fold)
Erlotinib [log]
C.
PC9
PC9 + Trap
PC9ER
PC9ER + Trap
Relative survival (fold)
Erlotinib [log]

639 **Figure 6**

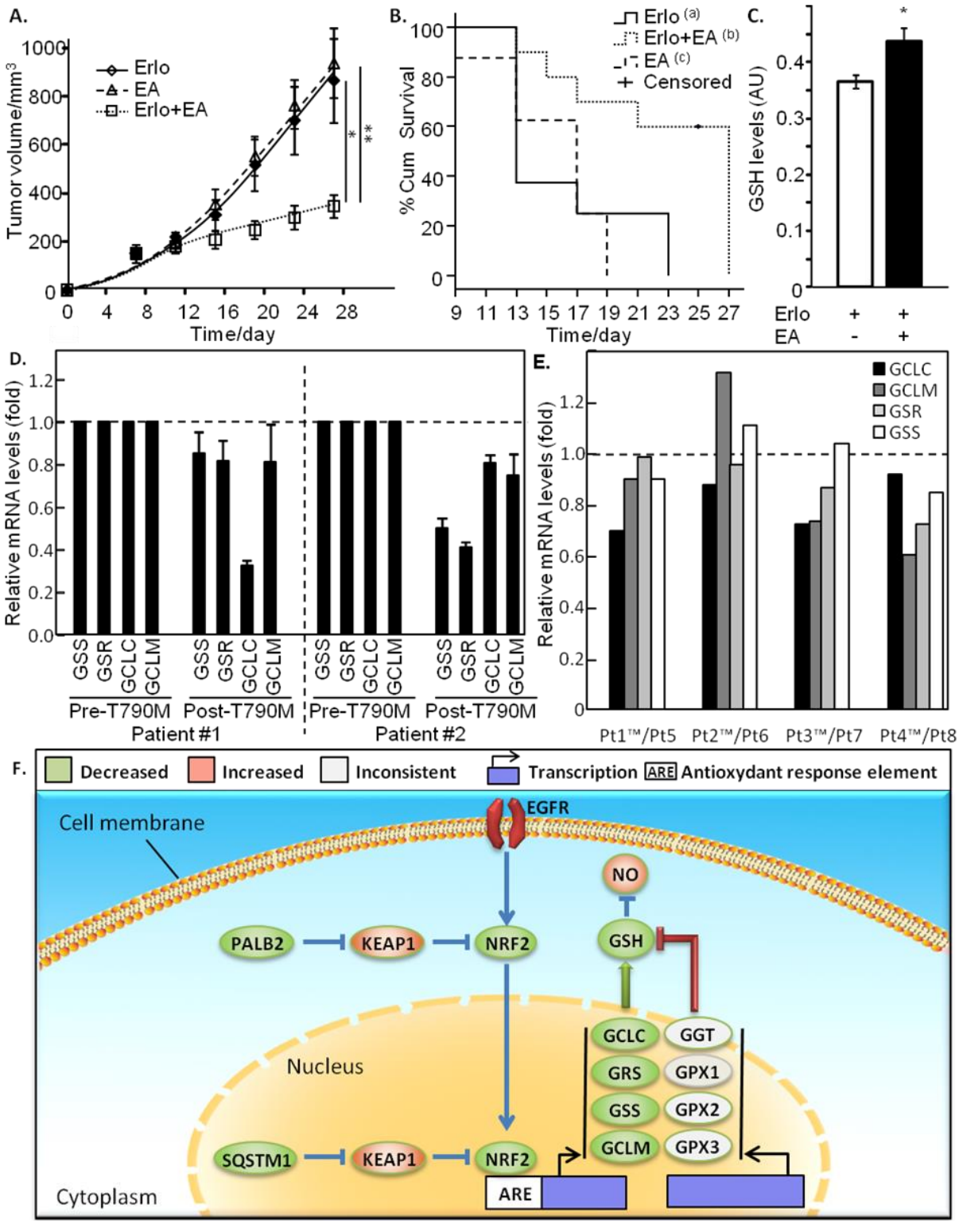

640

641

SUPPLEMENTARY TABLE AND FIGURE LEGENDS

SUPPLEMENTARY TABLES

Supplementary Table 1: Full list of the assigned metabolites identified through NMR-based metabolic profiling. Keys refer to the peaks labelled on **Figure 1A**. The chemical shifts for proton ($\delta^{1}H$) and carbon ($\delta^{13}C$) NMR are shown. [a] Multiplicity: singlet(s), doublet(d), triplet(t), quartet(q), doublet of doublets(dd), double of triplets (dt), multiplet(m). [b] The signals or the multiplicities were not determined.

Supplementary Table 2: List of shared metabolites similarly regulated in both cell line pairs between erlotinib-resistant and sensitive cells. Keys refer to the peaks labelled on **Figure 1B and C**. The chemical shifts for the identified metabolites and the OPLS-DA coefficient for both cell line pairs are shown.

SUPPLEMENTARY FIGURES

Supplementary Figure 1: (A and B) PC9ER and H1975 cells are resistant to the EGFR TKIs. PC9, PC9ER, H3255 and H1975 cells were treated with increasing concentrations of erlotinib (A) or 324674 (B) for 48 h before crystal violet staining. (C) PC9 and PC9ER cells do not display differential sensitivity to classical chemotherapeutic agents. PC9 and PC9ER cells were treated with increasing concentrations of cisplatin, taxol and etoposide for 48 hours prior to crystal violet staining. Results shown are representative of at least three independent experiments. Data are average ± SEM of quadruplicates.

Supplementary Figure 2: (A-C) Schematic representation of additional metabolic pathways differentially modulated in erlotinib-resistant and sensitive cells. Red; metabolites with increased and Blue; decreased levels in resistant cells as compared to their sensitive counterparts. **(D)** Representative ^{1}H-NMR spectra from the cell culture media of PC9, PC9ER, H3255 and H1975 cells. Cells were grown for 4 days in complete medium. The media were then collected and analysed by NMR for their GSH content. The spectra are zoomed onto the chemical shifts area corresponding to GSH and GSSG. The top line corresponds to a purchased GSH/GSSG mixture internal control. The spectra shown are representative of 10 replicates per cell lines.

Supplementary Figure 3: qPCR controls for siRNA-mediated silencing of GSH metabolic enzymes and accompanying changes in GSH levels. **(A)** PC9 and PC9ER cells were transfected with siRNAs targeting the indicated enzymes. 48 h later, transfected cells were subjected to RT-qPCR to assess the down-regulation of the target mRNAs. Data are shown are average of quadruplicates ± SEM. **(B)** GSH levels were measured by colorimetric assay in PC9 or PC9ER cells downstream of the silencing of selected targets. Data are shown are representative of at least three experiments. Results are average of

quadruplicates ± SEM. (B) Statistical analysis, Student *t*-test with NT taken as reference. *; $p \leq 0.05$, **; $p \leq 0.01$.

C) H1975 cells were transfected with siRNAs for the indicated enzymes or a non-targeting sequence (NT) prior to treatment with the IC_{50} concentration of erlotinib for H3255 cells. Cell survival was determined by crystal violet staining and normalised to that of the NT condition. **(D)** Intracellular GSH levels were measured in H1975 cells treated with or without MS using a colorimetric assay. **(E)** H1975 cells were incubated in the presence or absence of MS for 2 h prior to treatment with or without erlotinib for 48 h. Cell viability was assessed by crystal violet staining. Results shown are representative of experiments performed at least three times. Data are average of quadruplicates ± SEM. Statistical analysis: (C-D) ANOVA, (E) Student *t*-test. ***; $p \leq 0.001$, **; $p \leq 0.01$ *; $p \leq 0.05$.

Supplementary Figure 4: PC9ER cells treated or not with Ethacrynic Acid (EA) were exposed to varying doses of Gefitinib for 48 hours and cell survival monitored by crystal violet staining (**A**). Fold change in cell survival at the IC50 dose was determined and data normalised to the cell viability with Gefitinib alone (**B)**. Fold change in GSH was measured in cells treated or not with Gefitinib, EA or combination (**C**).

Supplementary Figure 5: Three replicates for the Western blots shown in Fig 4A and B were quantified using the optical densitometry function in ImageJ and the results obtained for **(A)** NRF2, **(B)** KEAP1, **(C)** SQSTM1 and **(D)** PALB2 normalised to the corresponding control cell line and plotted. (**E-F**) mRNA level of SQSTM1 was quantified for 4 cell lines and results were normalised to the corresponding control cell line. Results shown are representative of experiments performed at least three times. Data are average of triplicates ± SEM. For PC9ER, PC9 cells were used as control while for H1975, H3255 were used for normalisation. Statistical analysis; *t*-test. ***; $p \leq 0.001$, *; $p \leq 0.05$.

Supplementary Figure 6: (**A, C and E**) qPCR controls for silencing of NRF2, SQSTM1 and KEAP1 in the indicated cell lines. (**B, D and F**) Accompanying changes in the mRNA levels for GSH synthesising enzymes as determined by qPCR. Data shown are representative of at least three independent experiments. Results are average of quadruplicates ± SEM. Statistical analysis; ANOVA, *; $p \leq 0.05$, ***; $p \leq 0.001$.

Supplementary Figure 7: Silencing of PALB2 in PC9 cells does not modulate their sensitivity to erlotinib. (**A and B**) Cells were transfected with siRNA targeting PALB2 or with a non-targeting control for 48 h prior to exposure to a dose range of erlotinib for 2 days (A) or GSH levels measurements using a colorimetric assay (B). Cell survival was assessed using crystal violet staining. Results shown are representative of experiments performed in triplicate. Data are average of quadruplicates ± SEM.

Silencing of T790M-EGFR using selective siRNA does only modify EGFR expression in T790M-EGFR containing cells as assessed by qPCR. PC9 and PC9ER cells were transfected with non-targeting (NT) or two separate T790M-targeting siRNAs (**C and D**) and subjected to qPCR for EGFR using primers

detecting equally T790M and non-T790M EGFRs. Results shown are normalised to the corresponding NT condition. Statistical analysis; Student *t*-test, ***; $p \leq 0.001$.

(E) Response to erlotinib during systemic EA administration in PC9 mouse xenografts. Nude mice (n=10/condition) were injected subcutaneously with PC9 cells and treatment started when tumours reached 100 mm^3. Tumour volume was monitored for 2 weeks**.**

Supplementary Figure 1 **Related to Figure 1**

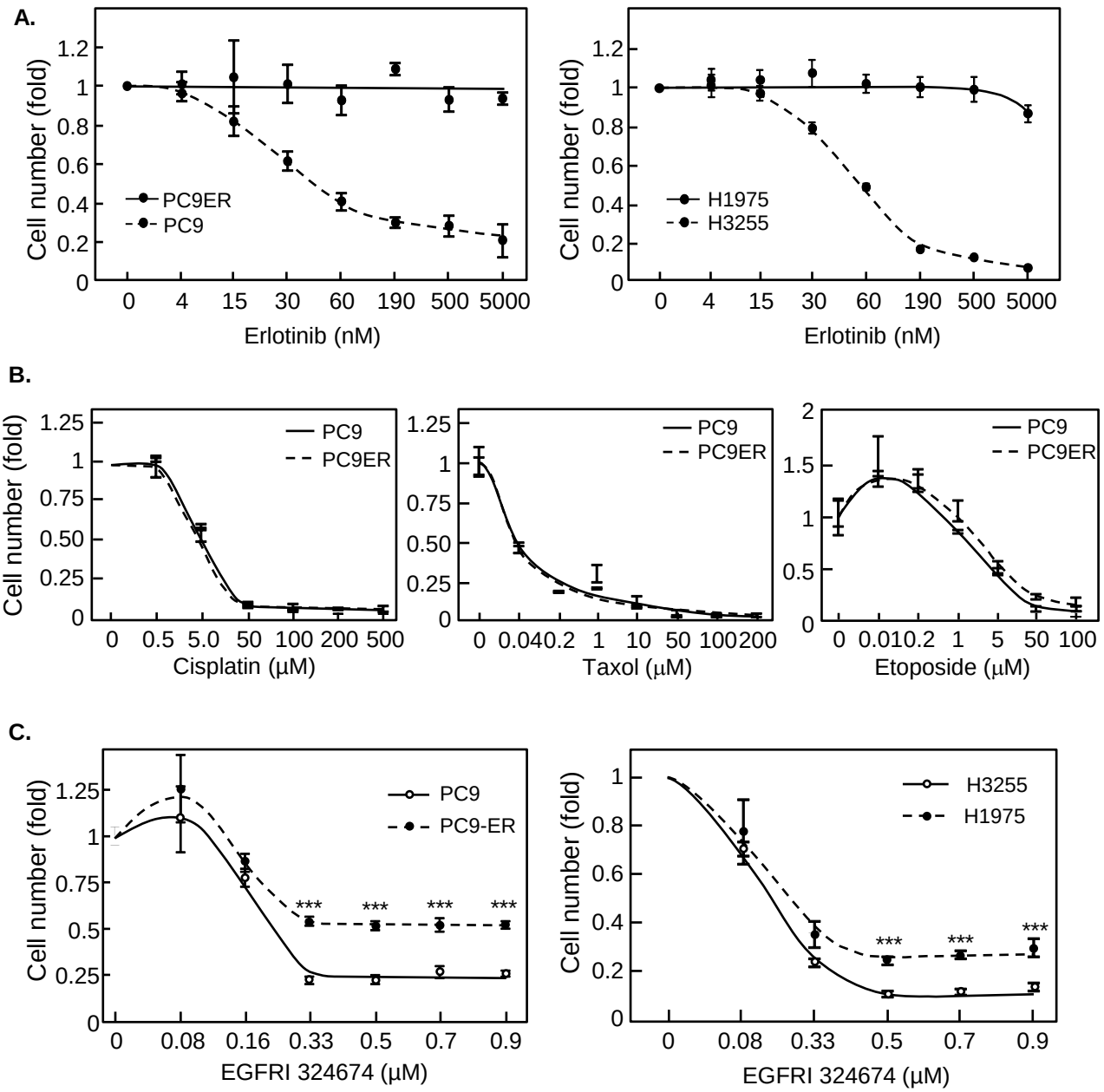

Supplementary Figure 2 **Related to Figure 2**

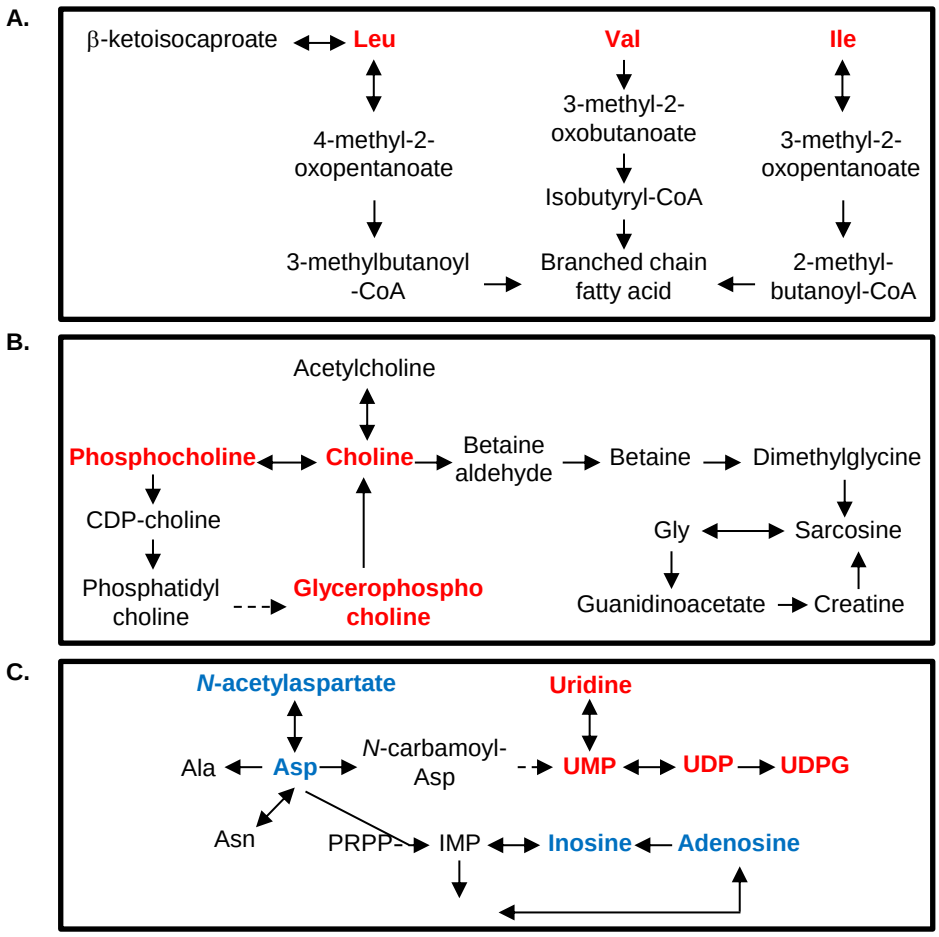

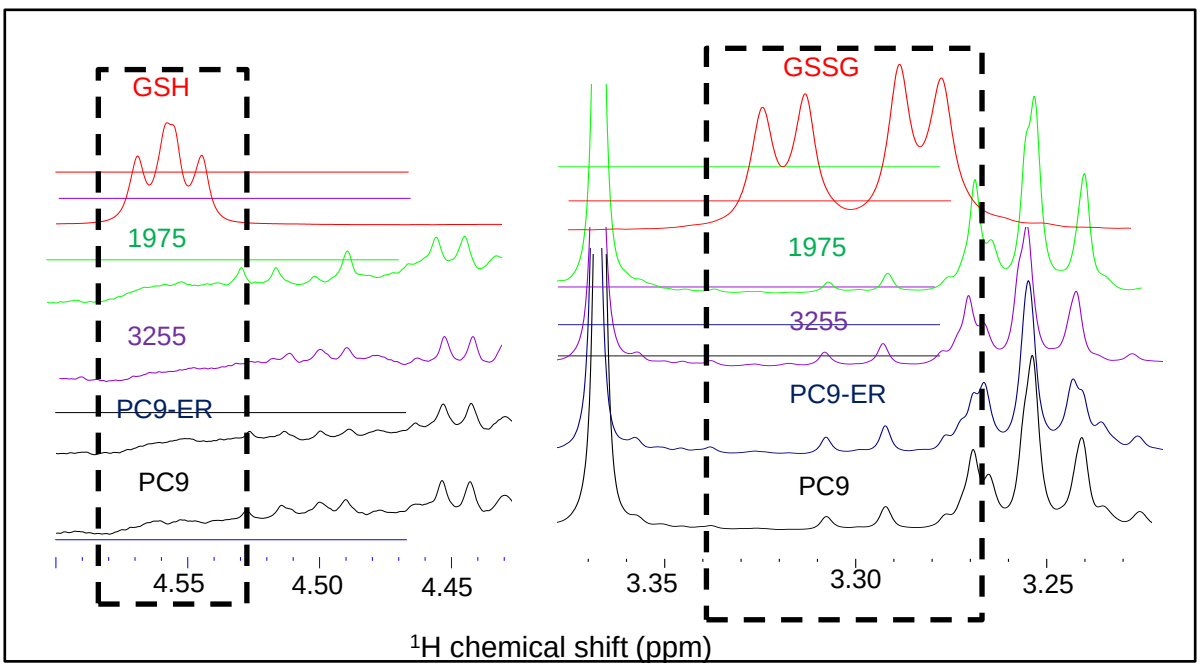

Supplementary Figure 3 **Related to Figure 2**

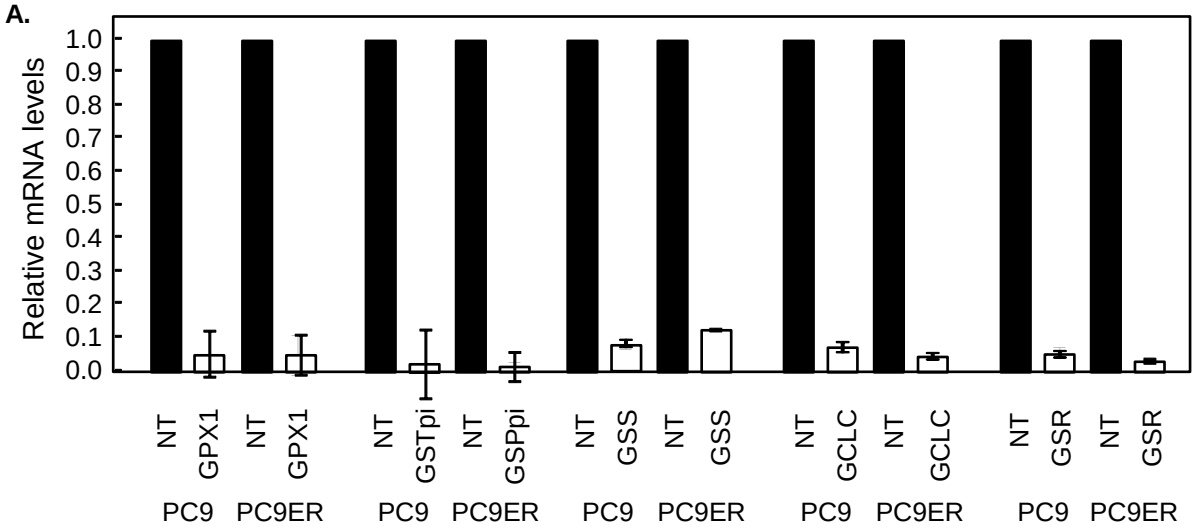

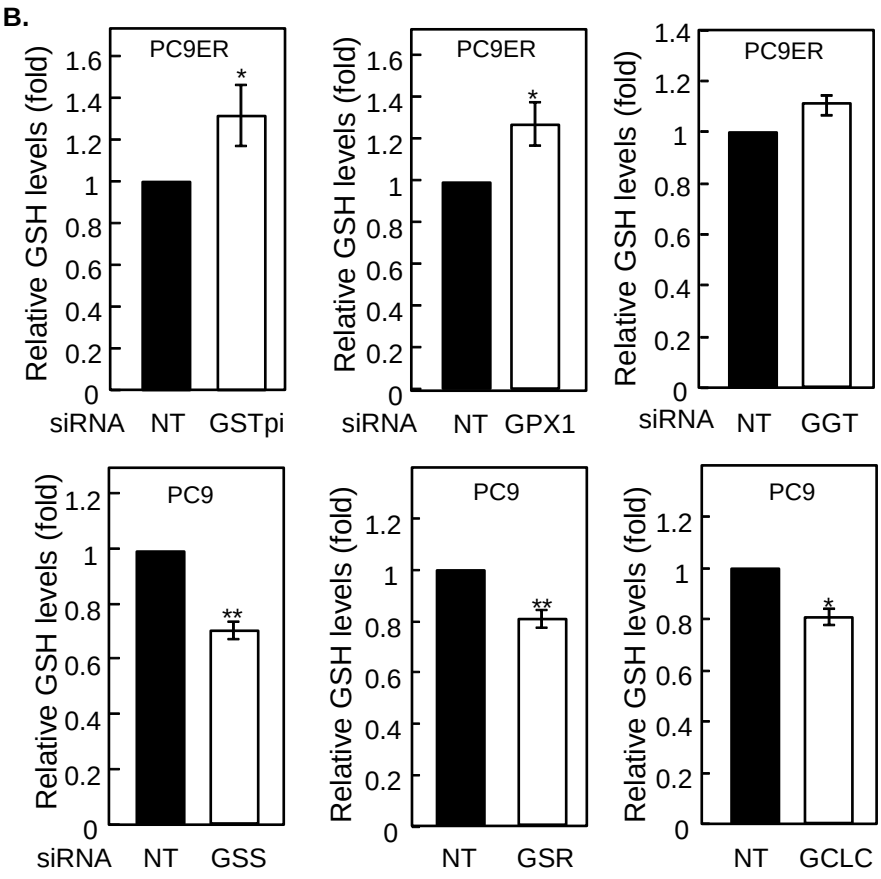

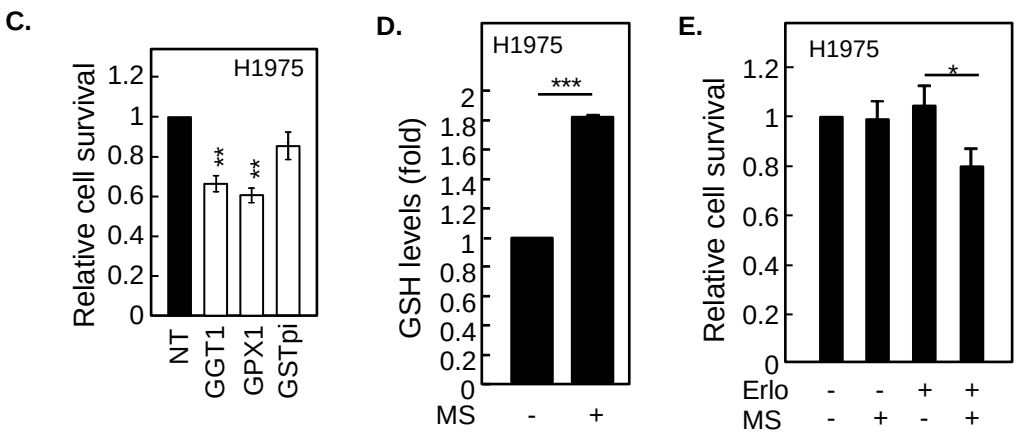

Supplementary Figure 4 **Related to Figure 2**

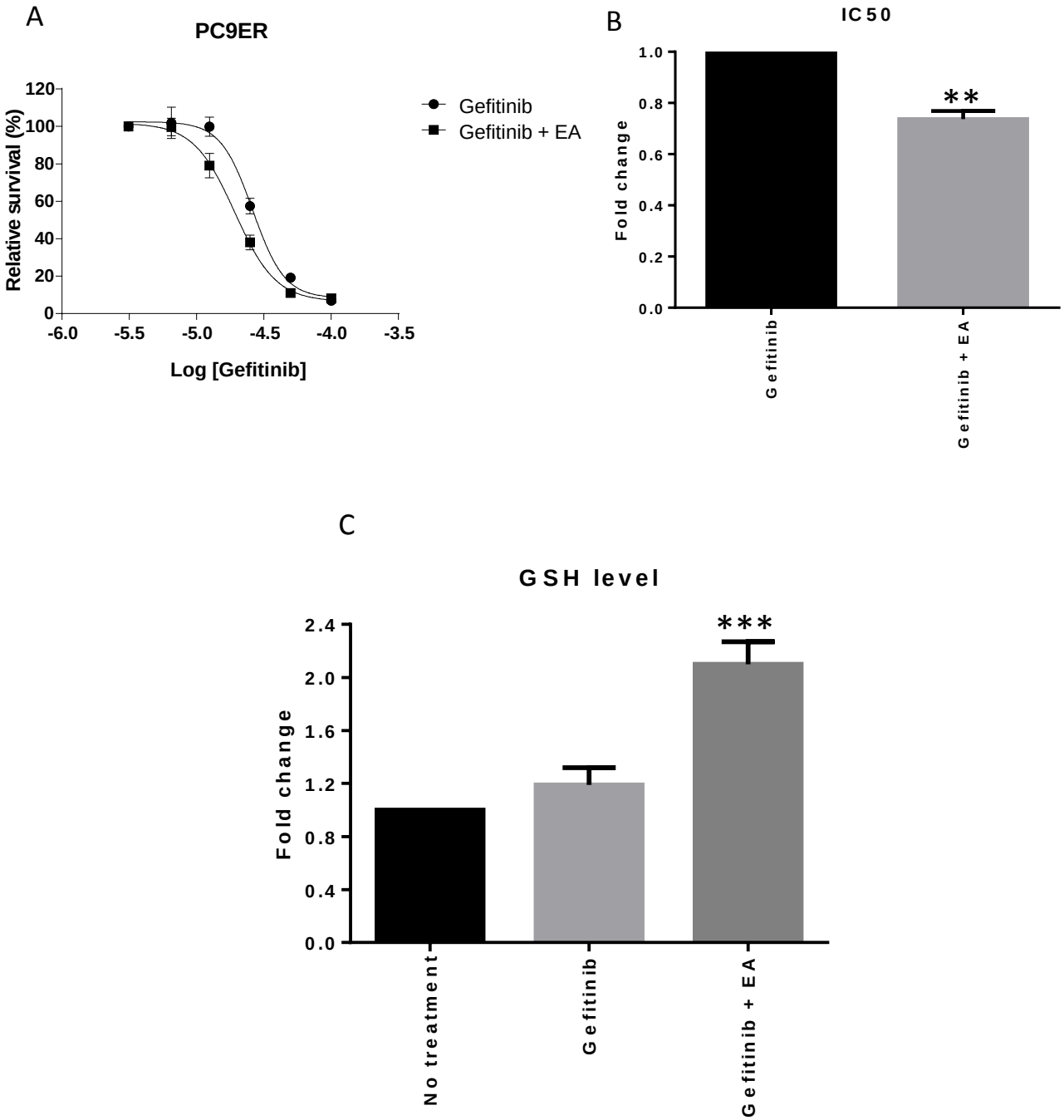

Supplementary Figure 5 **Related to Figure 3**

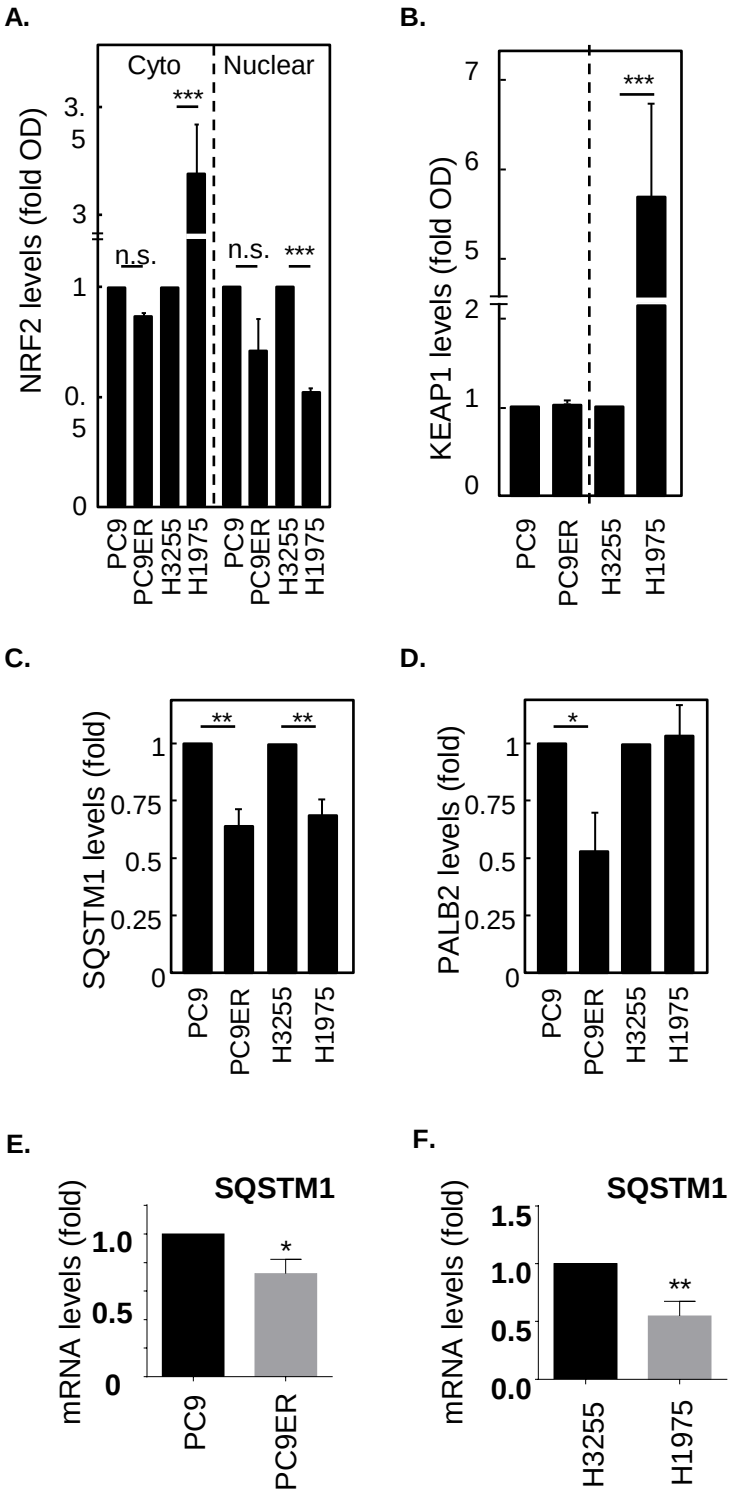

Supplementary Figure 6 **Related to Figure 3**

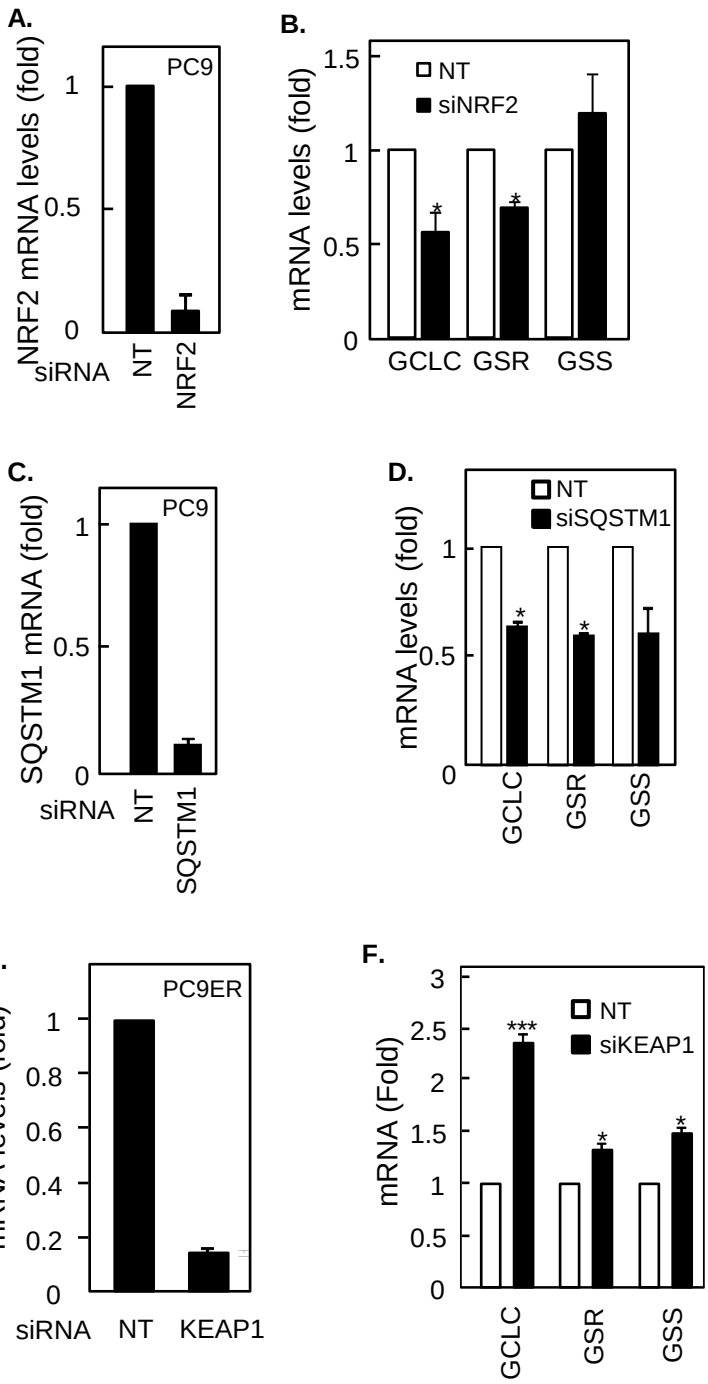

Supplementary Figure 7 **Related to Figure 4**